Winter 12-15-2014

Polyol Synthesis of Silver Nanowires by Heterogeneous Nucleation and Mechanistic Aspects Influencing its Length and Diameter

Waynie M. Schuette
Washington University in St. Louis

WASHINGTON UNIVERSITY IN ST. LOUIS

Department of Chemistry

Dissertation Examination Committee:
William E. Buhro, Chair
Victor Gruev
Richard A. Loomis
Kevin D. Moeller
Bryce Sadtler

Polyol Synthesis of Silver Nanowires by Heterogeneous Nucleation and Mechanistic Aspects Influencing its Length and Diameter

by

Waynie Mark Schuette

A dissertation presented to the
Graduate School of Arts & Sciences
of Washington University in
partial fulfillment of the
requirements for the degree
of Doctor of Philosophy

December 2014
St. Louis, Missouri

Table of Contents

List of Figures

Chapter 1: Introduction to Polyol Synthesis of Silver Nanowires

Chapter 2: Silver Chloride as a Heterogeneous Nucleant for the Growth of Silver Nanowires

Chapter 3: Polyol Synthesis of Silver Nanowires by Heterogeneous Nucleation; Mechanistic Aspects Influencing Nanowire Diameter and Length

Appendix A Additional Figures for Chapter 2

Appendix B Additional Figures for Chapter 3

List of Tables

Chapter 2: Silver Chloride as a Heterogeneous Nucleant for the Growth of Silver Nanowires

Chapter 3: Polyol Synthesis of Silver Nanowires by Heterogeneous Nucleation; Mechanistic Aspects Influencing Nanowire Diameter and Length

Appendix B Additional Figures for Chapter 3

List of Schemes

Acknowledgments

First and foremost, I would like to thank my advisor Professor Bill Buhro for his guidance, encouragement, education and patience throughout my graduate career. Thank you for taking the time to meet with me to discuss research and prepare manuscripts as often as I wished for, despite your busy schedule as a chair. Through the years you have constantly challenged me and helped me grow as a scientist. I am also especially grateful for your help accommodating me during both my pregnancies and for all your advice on parenthood.

I would also like to thank Professor Kevin Moeller and Professor Richard Loomis for helpful advice on my research. Thank you to my committee members Professor Victor Gruev and Professor Bryce Sadtler for taking the time to serve as members of my defense committee.

I would also like to thank past and present members in our group, Dr. Fudong Wang for training me on various instruments and experimental advice, Dr. Yuanyuan Wang and Dr. PJ Morrison for help in using instrumentation and lab members Linja Mu and Yang Zhou.

Thank you to my Mom and Dad for all their sacrifice, love and support and for working hard to help me pursue my goals without restrictions. I would like to thank my brother William for his never ending encouragement and his help getting me through my PhD years. Thank you to my sister Wega for being the best aunty to my kids. I would also like to thank my mother-in-law, father-in-law and Grandma Gunloh for their support and love.

And finally thanks to my husband Mark for going on this incredible journey with me and for your unwavering love. You have constantly encouraged me, endured my frustrations and enthusiastically celebrated my successes. I am also thankful and truly lucky to be a mom to the most wonderful kids in the world Jack and George.

Lastly I would like to thank Washington University for funding this project and providing me with the opportunity to pursue my research goals.

Waynie Mark Schuette

Washington University in St. Louis

December 2014

To Mark, Jack and George

ABSTRACT OF THE DISSERTATION

Polyol Synthesis of Silver Nanowires by Heterogeneous Nucleation and Mechanistic Aspects Influencing its Length and Diameter

by

Waynie Mark Schuette

Doctor of Philosophy in Chemistry

Washington University in St. Louis, 2014

Professor William E. Buhro, Chair

Various additives are employed in the polyol synthesis of silver nanowires (Ag NWs), which are typically halide salts such as NaCl. A variety of mechanistic roles have been suggested for these additives. My research showed that the early addition of NaCl in the polyol synthesis of Ag NWs from $AgNO_3$ in ethylene glycol results in the rapid formation of AgCl nanocubes, which induce the heterogeneous nucleation of metallic Ag upon their surfaces. Ag NWs subsequently grow from these nucleation sites. The conclusions are supported by studies using *ex-situ* generated AgCl nanocubes.

Additionally, the final mean silver nanowire diameter is found to be independent of the size of the heterogeneous nucleant, showing that the diameter is not significantly influenced by the nucleation event. Kinetics studies determine that nanowire diameter, length, and aspect ratio grow in parallel to one another and with the extent of the Ag^+ reduction reaction, demonstrating that growth is reduction-rate limited. The results are interpreted to support nanowire growth by a surface-catalyzed reduction process occurring on all nanowire surfaces, and to exclude nanoparticle aggregation or Ostwald ripening as primary components of the growth mechanism.

Chapter 1

Introduction to the Polyol Synthesis of Silver Nanowires

The polyol method is the most commonly used synthesis of silver nanowires (Ag NWs), yet major questions remain regarding the mechanism of growth and how the nanowire achieves its final length and diameter. Moreover, the use of halide additives such as NaCl are known to be necessary to achieve selectivity for nanowire growth, however their precise role was not determined prior to this study. Finally, Ag NW growth has been ascribed to Ostwald ripening or alternatively to nanoparticle aggregation by oriented attachment, but no mechanistic studies exist to support these proposed mechanisms.

In this study, halide additives like NaCl employed in the polyol synthesis of silver nanowires are shown to rapidly form AgCl nanocubes *in-situ*, which subsequently induce the heterogeneous nucleation of metallic Ag upon their surfaces. This is followed by the initiation of Ag NW growth from the surface-bound metallic Ag nanoparticles. Kinetic studies show that the diameter and length grow in parallel to one another and with the extent of the Ag^+ reduction reaction, demonstrating that the growth is reduction-rate limited. Additionally, Ostwald ripening and aggregative growth of Ag nanoparticles are shown to contribute insignificantly to Ag NW growth.

The earliest study of colloidal metallic nanoparticles dates back to the 1850s when Michael Faraday synthesized ruby-red Au particle suspensions[1] and studied the properties of these particles. He observed that when particle dimensions become smaller than that of wavelengths of visible light, they interact strongly with light. These earliest techniques to synthesize nanoparticles became the basis of modern nanoparticle synthetic methods. For example, Faraday synthesized the Au nanoparticle suspensions by reduction of gold chloride by phosphorous in carbon disulfide.[1] Creighton and coworkers [2] synthesized Ag nanoparticles by the reduction of $AgNO_3$ by $NaBH_4$. The polyol process was first developed by Figlarz and

coworkers[3] to prepare monodisperse Co and Ni nanoparticles by precipitation reactions in liquid polyols.

A unique aspect of nanoparticles that makes it very different from its bulk counterpart is their high surface to volume ratio, which affects chemical reactivity and some physical characteristics like melting point.[4] Metal nanoparticles like silver nanowires for example exhibit strong size-dependant plasmonic properties.[4]

1.1 Applications of Silver Nanowires

Materials with high electrical conductivity and optical transparency have been sought after to replace the traditional indium tin oxide (ITO) metal films for applications in devices like liquid crystal, flat planel or plasma displays, touch panels, organic light emitting diodes and solar cells.[5] Some problems with the ITO films currently used are the rising cost of indium, brittleness of ITO and the high temperatures required for its processing.[5] Silver nanowires networks have a promising future as transparent conducting films due to their high DC to optical conductivity ratios (σ_{DC}/σ_{Op}).[6,7] Graphene based films[8] have $\sigma_{DC}/\sigma_{Op} = 0.5$, while for nanotubes[9] $\sigma_{DC}/\sigma_{Op} = 25$, silver nanowire thin films were demonstrated to have $\sigma_{DC}/\sigma_{Op} = 500$.[6]

Silver nanowires are also potentially important in the field of complementary metal-oxide-semiconductor (CMOS) imaging devices. Polarization contrast imaging is useful in optically scattering environments like underwater imaging, foggy conditions etc.[10] A polarization image sensor will have a nanowire optical filter which will record the polarization property of light in real time.[10] An ideal nanowire for the dynamic polarization medium for the image sensor would be able to rapidly orient itself in an electric field and would be able to absorb light in the visible and UV - IR regions.[10] Silver nanowires were shown to spontaneously align on the

surface of water at the oil-water-air interface (Figure 1.1) and thus could be ideal candidates for the polarization-image sensor.[11]

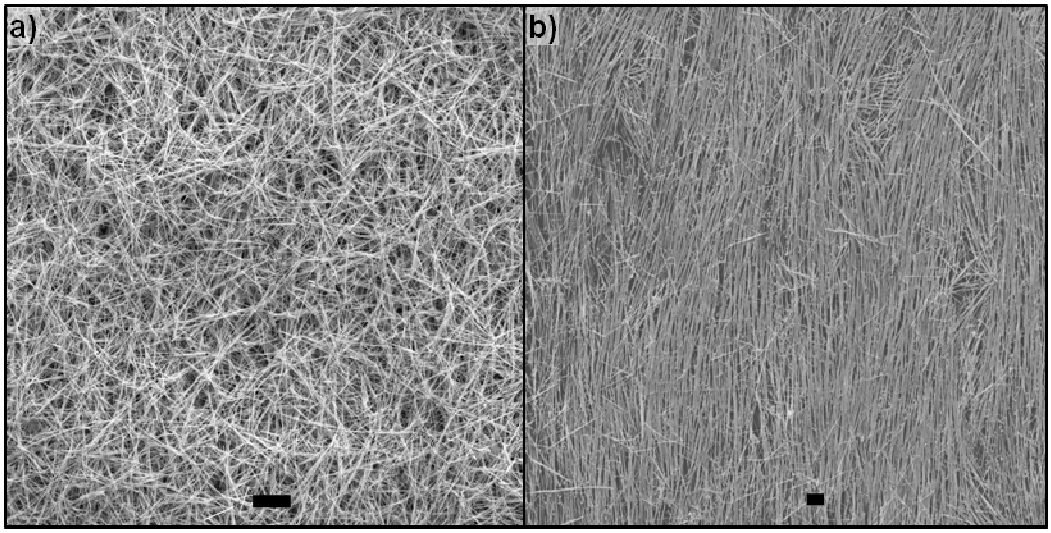

Figure 1.1 SEM image of (a) disordered Ag NWs and (b) Ag NW film formed on the surface of the oil-water-air interface showing aligned nanowires. The scale bars are 10 μm.

Silver nanoparticles exhibit surface plasmon resonance (SPR) which is the strong oscillation of free electrons on the surface of the nanoparticle in response to an electromagnetic radiation, resulting in strong absorption and scattering of light. As a result of the plasmonic coupling to the metal nanoparticle the raman spectrum (surface enhanced raman scattering) can be enhanced by several orders of magnitude,[12] large enough that even the raman spectrum of single molecules was acquired.[13] The large enhancement in the raman scattering property is useful in biosensors[14] and in plasmon-based photonic circuitry.[15]

Successful applications of nanoparticles depend on the ability to synthesize monodisperse nanoparticles and the ability to control the size and shape of these particles.[4] In

recent years, size and shape control of metal and semiconductor nanoparticles has been the focus of many research groups.[16-19]

1.2 Synthetic strategies of Silver Nanowires

Ag NWs have been grown using a variety of template strategies using hard templates like alumina,[20] carbon nanotubes[21] and mesoporous materials[22] and soft templates like DNA[23] and micelles.[24] Although some aspect-ratio control have been achieved using this template strategy, fabrication of the templates and harvesting the nanowires after the synthesis are often tedious and time consuming.

Murphy and coworkers[25] demonstrated the aqueous synthesis of Ag NW and nanorods (NRs) by the reduction of silver precursor, $AgNO_3$ and in the presence of capping agent cetyltrimethylammonium bromide (CTAB) and silver seeds. Silver seeds (Average diameter ~4 nm) were initially synthesized and then added to reaction mixture containing the silver precursor and capping agents. Various capping agents like tetrabutylammonium bromide[26] and sodium dodecyl sulfate,[27] dodecyl benzene sulfonic acid[28] were used in the synthesis of Ag NWs. In the aqueous synthesis, Ag NWs were made in high yields; however, there was no good method to control aspect ratios (ranged from 50-350).[29] The solution-based polyol synthesis of Ag NWs (see below) especially the one-pot-strategy popularized by Xia and coworkers[31] is the most commonly used method to synthesize Ag NWs with the highest yields and largest aspect ratios.

1.3 Polyol synthesis of Silver Nanowires

The polyol process is based on the high temperature reduction of an inorganic salt in the presence of a surfactant, where the polyol acts as the reductant and the surfactant prevents agglomeration and helps in stabilizing the nanoparticles formed. The polyol process was first

studied by Figlarz and coworkers[3] for cobalt, copper, nickel, silver, gold, palladium, iron-nickel alloy and other precious metals. The group first synthesized Ag nanorods and Ag NWs (Figure 1.2) in 1992 using ethylene glycol as the solvent and reductant, polyvinylpyrrolidone (PVP) as the capping agent, and $AgNO_3$ as the silver precursor. The reactions with the largest yields were run at 160 ºC for ~15 mins.

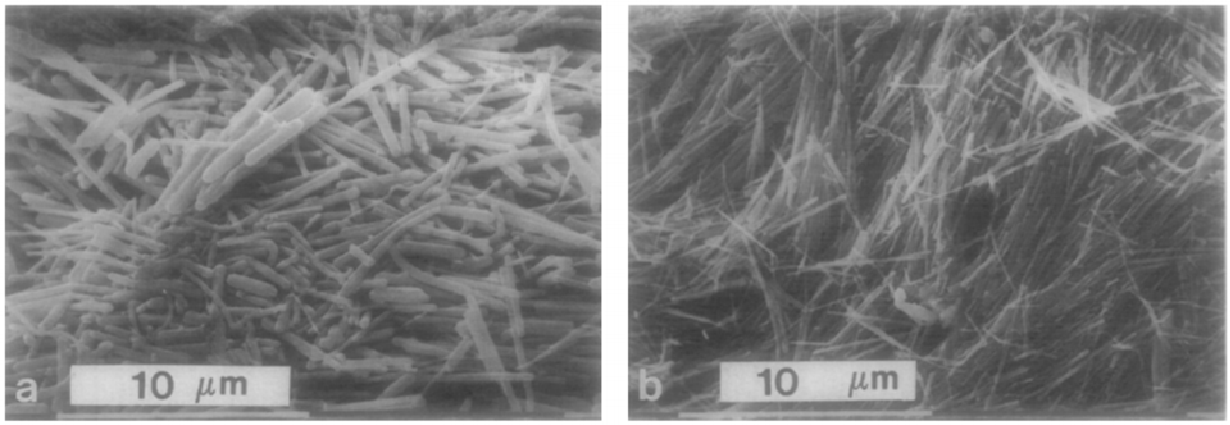

Figure 1.2 Microphotographs of silver nanorods and Ag NWs synthesized by Figlarz and coworkers using different PVP:$AgNO_3$ ratios (a) 1:1 and (b) 4:1. Reprinted from ref 30. Copyright 1992, with permission from Elsevier.

The authors discussed both homogeneous and heterogeneous growth mechanisms for the Ag NWs. In case of a homogeneous growth mechanism, the Ag NWs grow from silver nuclei formed initially in the hot reaction mixture, while in case of heterogeneous nucleation, Ag NWs grow from platinum nuclei that form from the reduction of hexachloroplatinic acid.[30]

1.4 Mechanism of growth of Silver Nanowires by the polyol process

Over the years many aspects of the mechanism of the polyol synthesis were elucidated. For example, Xia and coworkers studied the growth and factors influencing formation of Ag NWs in solution in detail. Using a simple spectroscopic test, the group showed that glycolaldehyde is the actual reductant for the Ag^+ ions in solutions.[31] The oxidation products

glycolic and oxalic acid were detected using HPLC showing that glycolic acid is the dominant product of the Ag^+ ion reduction reaction in ethylene glycol.[32] If glycolaldehyde was indeed the Ag^+ reductant in the polyol synthesis, then its addition to the reaction mixture should affect the reduction kinetics. This hypothesis was tested in Chapter 3. We show that the slow adventitious generation of glycolaldehyde by the air oxidation of ethylene glycol under reaction conditions is the reason for the slower reduction kinetics (at lower temperatures) and the presence of an induction period prior to the commencement of nanowire growth. Additionally, in the presence of excess glycolaldehyde in solution, the reduction reaction is no longer temperature dependant.

Figlarz and coworkers[30] showed that the addition of PVP is essential to obtaining Ag NWs as they prevented the coalescence of the nuclei during the initial growth step of the Ag NWs. Shape control of silver nanostructures[33] was shown by the varying the $AgNO_3$ concentrations in solution and ratios of PVP: $AgNO_3$. PVP was shown in several studies to preferentially bind to the side (100) facet of the growing Ag NW thus enabling anisotropic growth of the multiply twinned particle.[34,35] Evidence for this preferential binding was shown by attaching Au nanoparticles to the tips of Ag NWs through a dithiol linkage.[34] The side facets of the Ag NWs remained too strongly passivated by the PVP to be replaced by the dithiol molecules. In contradiction, it was shown by Kitaev et al.[36] that PVP does not preferentially bind to any specific facet. The authors claimed that PVP was crucial for colloidal nanoparticle stabilizing and facet preservation through steric protection.[36] Although it was proposed that the diameter of the Ag NW does not increase due to strong passivation by PVP on the side facets of the growing NW, in Chapter 3 we show that the diameter of Ag NW increase throughout the Ag^+ reduction process and is not fixed at the nucleation event.

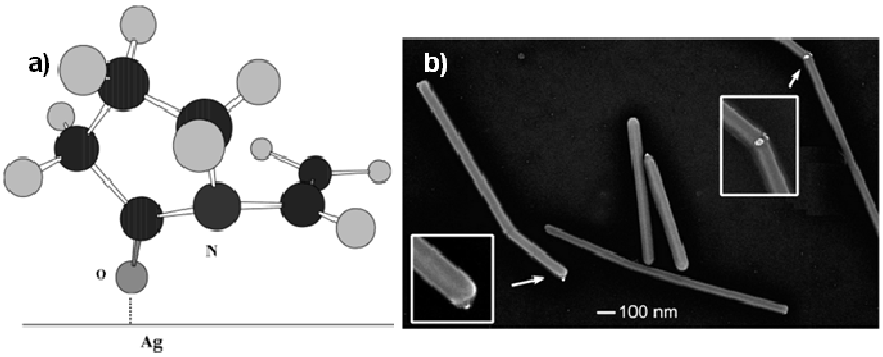

Figure 1.3 (a) Cartoon illustration of proposed binding of PVP (by Ag:O coordination) on the surface of Ag NWs. Reprinted with permission from ref 37. Copyright 2004, American Chemical Society. (b) SEM image of Ag NWs with Au nanoparticles attached to its tip facets by dithiol linkage. Reprinted with permission from ref 34. Copyright 2003, American Chemical Society.

Metal halides, such as $PtCl_2$,[38] AgCl,[39] NaCl,[40] *etc.*, are often added and found to be crucial to the formation of NWs. Figlarz and coworkers proposed that the Pt seeds act as heterogeneous nucleants for the Ag NWs.[30] It was also shown that the chloride ion selectively etches away initially formed multiply twinned Ag particles in the presence of oxygen, [41] which was proposed to either hinder,[42] or promote[43] Ag NW formation. The most commonly accepted explanation for the role of the Cl^- ions is to provide electrostatic stabilization, preventing nanoparticle agglomeration and promoting Ag-NW growth.[44] In Chapter 2 we show that the sodium chloride additive forms AgCl nanocubes *in situ* which then act as heterogeneous nucleants for the Ag NW growth. Control experiments with the addition of pre-synthesized AgCl nanocubes also showed Ag NWs growing out of the surfaces of the AgCl nanocubes.

Immediately following the addition of the $AgNO_3$ and PVP into the hot ethylene glycol reaction mixture, silver clusters form that convert to five-fold multiply twinned particles once they reach a critical size.[45] Marks showed that single-crystal Ag nanoparticles transition to multiply twinned particles only after they grow beyond a critical size of 10 nm (*in vacuo*).[45] Although the formation of the multiply twinned particle is energetically favorable, the twin

planes are high energy sites. It was previously shown[34] that once formed *in situ*, the multiply twinned particles rapidly grow anisotropically by the addition of Ag^+ atoms to both the tip facets of the growing Ag NW (Figure 1.3). Xia and coworkers claimed that Ostwald ripening is the mechanism of growth of the Ag NWs.[34] Ag NWs grown by reduction in N,N – dimethylformamide were thought to grow through the coalescence of silver nanocrystals in solution through an aggregative growth mechanism.[46] Contrary to previously proposed mechanisms of growth of Ag NWs, in Chapter 3 we show that silver nanowire growth is surface reduction-rate limited on all nanowire surfaces, and excludes nanowire growth by nanoparticle aggregation or Ostwald ripening.

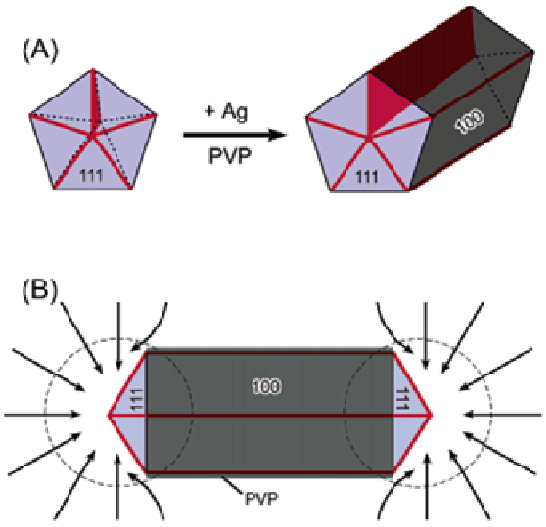

Figure 1.4 Cartoon illustration depicting (a) the growth of Ag NWs from a multiply twinned particle and (b) the addition of Ag^+ to the tip-(111) facets of the growing Ag NW. Reprinted with permission from ref 34. Copyright 2003, American Chemical Society.

1.5 How to control the length and diameter of silver nanowires?

In the aqueous synthesis of Ag NWs, Murphy and coworkers[25] showed that control of the aspect ratio of Ag NWs was possible by varying the amount of NaOH in solution. Silver nanorods were synthesized a higher NaOH concentration (Figure 1.5a) and Ag NWs were

synthesized at a lower NaOH concentration (Figure 1.5b). At higher amounts of NaOH, and at higher pH, the ascorbate dianion influenced growth kinetics while at lower amounts of NaOH and at lower pH, the monoanion of ascorbic acid influenced growth kinetics.

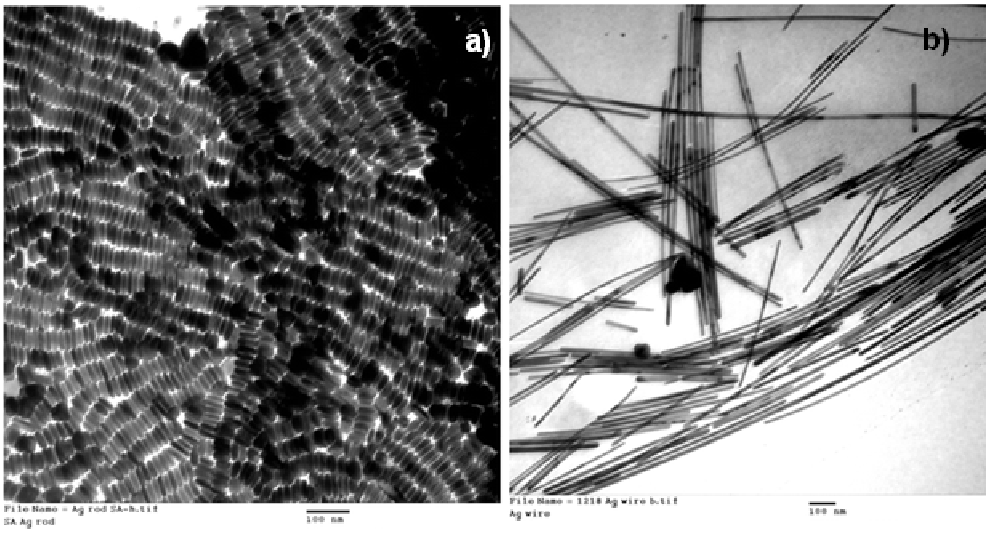

Figure 1.5 SEM images from aqueous synthesis of (a) Ag nanorods at higher NaOH concentrations and (b) Ag NWs at lower NaOH concentrations. Reproduced from ref. 25 with permission from The Royal Society of Chemistry.

Wiley and coworkers[47] proposed that control the length and diameter of the Ag NWs was possible simply by varying reaction temperature and total reaction time (Figure 1.6a) of the polyol synthesis. At lower temperatures, the nucleation rate was lower (and with the same amount of precursor as in higher temperature case) which resulted in longer and thicker wires compared to the higher temperature case, where the nucleation rate was high, resulting in shorter and thinner wires.[47]

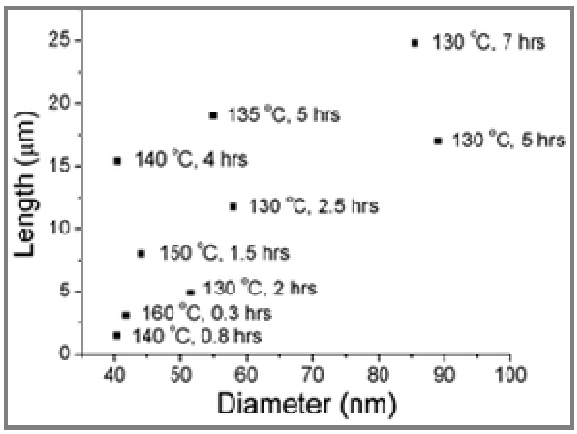

Figure 1.6 Plot showing (a) the temperature and reaction-time dependence on the aspect ratio of Ag NWs grown by the polyol process. Reproduced from ref. 47 with permission from The Royal Society of Chemistry.

Chou et al.[48] showed that as the chloride ion concentration in solution increased, the Ag NWs diameter decreased in the polyol process. The authors proposed that as more chloride ions bound to the side facets of the growing Ag NWs, the diameter of the wires decreased. The surface poisoning strategy was also used to control the diameter of Ag NWs in other studies that varied the concentration of PVP in solution. For example at higher PVP concentrations, thinner wires were obtained (Figure 1.2).[30,38]The excess adsorption of PVP to the side facets of the growing Ag NWs inhibited growth in the side (100) facets. Conversely, Jiang and coworkers[49] showed that when the concentration of Na_2S increased in solution, Ag NW-diameters increased which the authors attributed to the ability of the Ag_2S colloids formed in solution to control the release of Ag^+ ions.

To achieve the control of aspect ratios of Ag NWs through the polyol synthesis, it is important to understand roles of all additives as well as mechanisms limiting the growth kinetics. The role of the halide additive in the polyol synthesis is explored in Chapter 2, which discusses how the addition of the halide additive results in the formation of AgCl nanocubes in solution which then heterogeneously nucleates the Ag NWs on its surfaces. Having discovered that the

AgCl nanocube serves as a heterogeneous nucleant, we considered the possibility of controlling the final diameters of the Ag NWs by varying the edge length of the AgCl nanocubes. However in Chapter 3 we show that the diameter of the Ag NWs has no relationship to the size of the AgCl nanocube. The diameter of the Ag NW was shown to continue to increase until the reduction reaction is complete. Next we sought to understand how the Ag NWs achieve its final length and diameter by studying mechanism limiting the growth of Ag NWs. Chapter 3 describes in detail the reduction and growth kinetics and the various factors limiting the growth of Ag NWs. Results presented support the conclusion that the polyol synthesis of Ag NWs is a rate-limiting surface-catalyzed Ag^{+} reduction reaction.

1.6 References

1. Faraday, M. *Philos. Trans. R. Soc. London* **1857**, *147*, 145 – 181.
2. Creighton, J. A.; Blatchford, C. G.; Albrecht, M. G. *J. Chem. Soc. Farad.Trans. II* **1979**, *75*, 790 – 798.
3. Fievet, F.; Lagier, J. P.; Blin, B.; Beaudoin, B.; Figlarz, M. *Solid State Ionics* **1989,** *32*, 198-205.
4. Daniel, M. C.; Astruc, D. *Chem. Rev.* **2004**, *104*, 293-346.
5. Kumar, A.; Zhou, C. *ACS Nano* **2010**, *4*, 11-14.
6. De, S.; Higgins, T. M.; Lyons, P. E.; Doherty, E. M.; Nirmalraj, P. N.; Blau, W. J.; Boland, J. J.; Coleman, J. N. *ACS Nano* **2009**, *3*, 1767-1774.
7. Lee, J. Y.; Connor, S. T.; Cui, Y.; Peumans, P. *Nano Lett.* **2008**, *8*, 689-692.
8. Wang, X.; Zhi, L. J.; Mullen, K. *Nano Lett*. **2008**, *8*, 323-327.
9. Geng, H. Z.; Lee, D. S.; Kim, K. K.; Han, G. H.; Park, H. K.; Lee, Y. H. *Chem. Phys. Lett*. **2008**, *455*, 275-278.
10. Gruev, V.; Van der Spiegel, J.; Engheta, N. Advances in Integrated Polarization Imaging Sensors, IEEE/NIH Life Science Systems and Applications Workshop, **2009**, 62-65.
11. Shi, H. Y.; Hu, B.; Yu, X. C.; Zhao, R. L.; Ren, X. F.; Liu, S. L.;Yu, S. H. *Adv. Funct. Mater*. **2010**, *20*, 958-964.
12. Moskovits, M. *Rev. Mod. Phys*.**1985**, *57*, 783.
13. Xu, H.; Aizpurua, J.; Käll, M.; Apell, P. *Phys. Rev. E* **2000**, *62*, 4318.
14. T.J. Silva, T. J.; Schultz, S. *Rev. Sci. Instrum*. **1996**, *67*, 715 -725.
15. Ditlbacher, H.; Hohenau, A.; Wagner, D.; Kreibig, U.; Rogers, M.; Hofer, F.; Aussenegg, F. R.; Krenn, J. *Phys. Rev. Lett*. **2005**, *95*, 257403.

16. Kongkanand, A.; Tvrdy, K.; Takechi, K.; Kuno, M.; Kamat, P. V. *J. Am.Chem. Soc.* **2008**, *130*, 4007-4015.

17. Jana, N. R.; Chen, Y.; Peng, X. *Chem. of Mater.* **2004**, *16*, 3931-3935.

18. Sun, Y.; Xia, Y. *Science* **2002**, *298*, 2176-2179.

19. Borgohain, K.; Singh, J. B.; Rao, M. R.; Shripathi, T.; Mahamuni, S. *Phys. Rev. B* **2000**, *61*, 11093.

20. Zhang, Z.; Gekhtman, D.; Dresselhaus, M. S.; Ying, J. Y. *Chem. Mater.* **1999**, *11*, 1659−1665.

21. Ugarte, D.; Chatelain, A.; de Heer, W. A. *Science* **1996**, *274*, 1897−1899.

22. Han, Y. J.; Kim, J. M.; Stucky, G. D. *Chem. Mater.***2000**, *12*, 2068−2069.

23. Braun, E.; Eichen, Y.; Sivan, U.; Ben-Joseph, G. *Nature* **1998**, *391*, 775−778.

24. Reches, M.; Gazit, E. *Science* **2003**, *300*, 625−627.

25. Jana, N. R.; Gearheart, L.; Murphy, C. J. *Chem. Commun.* **2001**, 617−618.

26. Kim, S. H.; Choi, B. S.; Kang, K.; Choi, Y.-S.; Yang, S. I. *J. Alloys Compd.* **2007**, *433*, 261.

27. Zheng, X.; Zhu, L.; Yan, A.; Wang, X.; Xie, Y. *J. Colloid Interface Sci.* **2003**, *268*, 357.

28. Zhou, G.; Lu, M.; Yang, Z.; Zhang, H.; Zhou, Y.; Wang, S.; Wang, S.; Zhang, A. *J. Cryst. Growth* **2006**, *289*, 255.

29. Caswell, K. K.; Bender, C. M.; Murphy, C. J. *Nano Lett.* **2003**, *3*, 667 – 669.

30. Ducamp-Sanguesa, C.; Herrera-Urbina, R.; Figlarz, M. *J. of Solid. State Chem.* **1992**, *100*, 272-280.

31. Skrabalak, S. E.; Wiley, B. J.; Kim, M.; Formo, E. V.; Xia, Y. *Nano Lett.* **2008**, *8*, 2077-2081.

32. Bock, C.; Paquet, C.; Couillard, M.; Botton, G. A.; MacDougall, B. R. *J. of the Amer. Chem. Soc.* **2004**, *126*, 8028-8037.

33. Wiley, B.; Sun, Y.; Mayers, B.; Xia, Y. *Chem.-A Eur. J.* **2005**, *11*, 454-463.

34. Sun, Y.; Mayers, B.; Herricks, T.; Xia, Y. *Nano Lett.* **2003**, *3*, 955-960.

35. Gao, Y.; Jiang, P.; Song, L.; Liu, L.; Yan, X.; Zhou, Z.; Xie, S. *J. of Phys D: Appl. Phys.* **2005**, *38*, 1061.

36. Murshid, N.; Kitaev, V. *Chem. Commun.* **2014**, *50*, 1247-1249.

37. Gao, Y.; Jiang, P.; Liu, D. F.; Yuan, H. J.; Yan, X. Q.; Zhou, Z. P.; Shen, D. Y. *J. of Phys. Chem. B* **2004**, *108*, 12877-12881.

38. Sun, Y.; Yin, Y.; Mayers, B. T.; Herricks, T.; Xia, Y. *Chem. Mater*. **2002**, *14*, 4736-4745.

39. Hu, L.; Kim, H. S.; Lee, J.-Y.; Peumans, P.; Cui, Y. *ACS Nano*. **2010**, *4*, 2955-2963.

40. Tsuji, M.; Matsumoto, K.; Jiang, P.; Matsuo, R.; Tang, X.-L.; Kamarudin, K. S. N. *Colloids Surf. A* **2008**, *316*, 266-277.

41. Korte, K. E.; Skrabalak, S. E.; Xia, Y. *J. Mater. Chem*. **2008**, *18*, 437-441.

42. Wiley, B.; Herricks, T.; Sun, Y.; Xia, Y. *Nano Lett.* **2004**, *4*, 1733-1739.

43. Gou, L.; Chipara, M.; Zaleski, J. M. *Chem. Mater*. **2007**, *19*, 1755-1760.

44. Wiley, B.; Sun, Y.; Xia, Y. *Acc. Chem. Res.* **2007**, *40*, 1067-1076.

45. Marks, L. D. *Ultramicroscopy* **1985**, *18*, 445-452.

46. Giersig, M.; Pastoriza-Santos, I.; Liz-Marzán, L. M. *J. of Mater. Chem.* **2004**, *14*, 607-610.

47. Bergin, S. M.; Chen, Y. H.; Rathmell, A. R.; Charbonneau, P.; Li, Z. Y.; Wiley, B. J. *Nanoscale*, **2012**, *4*, 1996-2004.

48. Chang, Y. H.; Lu, Y. C.; Chou, K. S. *Chem. Lett.* **2011**, *40*, 1352-1353.

49. Chen, D.; Qiao, X.; Qiu, X.; Chen, J.; Jiang, R. *J. of Colloid and Interface Science*, **2010**, *344*, 286-291.

Chapter 2

Silver Chloride as a Heterogeneous Nucleant for the Growth of Silver Nanowires

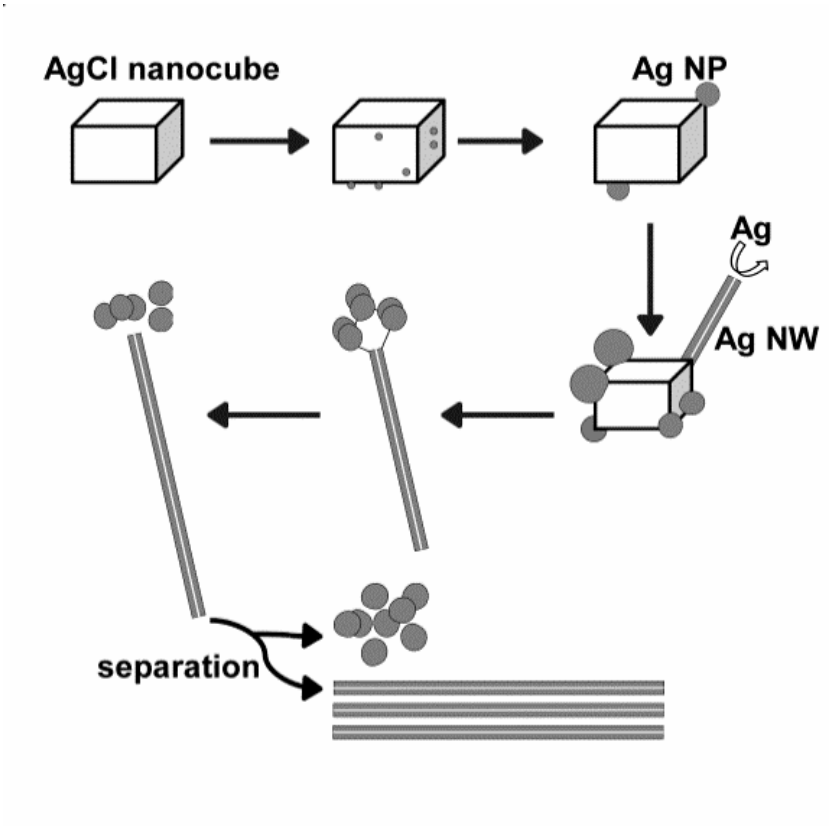

2.1 Introduction

Silver nanowires (Ag NWs) have received much interest in recent years due to their electronic and optical properties.[1-3] Straightforward, high-yield syntheses of one-dimensional Ag nanostructures are now available,[4-9] and Ag NWs are typically prepared by the polyol method.[10-23] Although much progress has been made on elucidating mechanistic aspects of the polyol synthesis of Ag NWs,[11,14-19,22,24] the role of the various additives employed remain unclear. In this chapter, we show that the additive NaCl is rapidly converted to AgCl nanocubes under the conditions of the polyol synthesis. The AgCl nanocubes subsequently induce heterogeneous nucleation of metallic silver on their surfaces, initiating growth of Ag NWs. A detailed understanding of this heterogeneous-nucleation process may ultimately lead to rational control of Ag-NW diameters, diameter distributions, and aspect ratios.

In the polyol process, silver nitrate is titrated into a mixture of hot (150-180 °C) ethylene glycol and polyvinylpyrolidone (PVP). The ethylene glycol serves as both the solvent and reducing agent, and PVP as the surfactant.[24] Various additives, such as $PtCl_2$,[11,13,15,18] AgCl,[28] NaCl,[18,20,22,23,25-27] ,AgBr[29] *etc.*, are also commonly employed and found to be crucial to the selective formation of NWs.[22] In some studies, initial reduction of the additives to homogeneous (Ag)[10,12] or heterogeneous (*e.g.* Pt)[11,13,15,17] seeds were proposed, which subsequently promoted the growth (on Ag seeds) or heterogeneous nucleation (on Pt seeds) of the Ag NWs.

Other studies claim that the halide component of the above additives is the species that controls Ag-nanoparticle morphologies. In some, chloride ion is shown to selectively etch away multiply twinned Ag particles in the presence of oxygen, [19,25,26,30] which is proposed to hinder,[25] or, conversely, to promote[20] Ag NW formation. The equilibrium reaction of Ag^+ and Cl^- (from NaCl) to form AgCl has been proposed to buffer the Ag^+-ion concentration, limiting Ag

nucleation events and thereby promoting the growth of Ag NWs.[20,21] Adsorption of Cl^- ions to Ag nanoparticle surfaces has also been proposed to provide electrostatic stabilization, preventing nanoparticle agglomeration and promoting Ag-NW growth.[7,14,19,25,26,30] In two studies, AgCl nanoparticles have been referred to as "seeds," but the precise role of the seeds was left unclear. To date, a heterogeneous-nucleation pathway involving AgCl nanoparticles has not been elucidated. Clearly, a mechanistic study that conclusively identifies the function of a NW-growth-promoting additive is desirable, given the wide variety of roles that have been proposed.

In this study, we monitored the polyol synthesis of Ag NWs employing NaCl as the growth-promoting additive. A combination of spectroscopy, microscopy, and x-ray diffraction (XRD) allowed us to determine the sequence of chemical, nucleation, and growth events occurring in the process. The detailed pathway was elucidated, which features the heterogeneous nucleation of Ag on *in-situ* generated AgCl nanocubes as a prominent event. Control experiments were also conducted to establish this heterogeneous nucleation as the origin of the Ag NWs produced. An analogy to photographic processing using silver halide emulsions, and insights into optimizing Ag-NW growth are also discussed.

2.2 Experimental

2.2.1 General Methods

All syntheses were conducted under ambient conditions. Anhydrous ethylene glycol (99.8%, Aldrich), ethylene glycol (>99.0 %, J. T. Baker), $AgNO_3$ (99+%, Aldrich), polyvinylpyrrolidone (PVP, MW ≈ 55,000, Aldrich), sodium chloride (99+%, Aldrich), ammonium hydroxide (28.0 – 30.0 w/w %, Fisher Scientific), and acetone (reagent grade, Aldrich) were used as received without further purification. Si(111) wafers were purchased from Aldrich. Deionized water was used in all procedures.

AgCl nanocubes were prepared according to a previously reported method.[31] The white precipitate obtained from the synthesis [31] was then washed with water and acetone to remove the excess ethylene glycol and PVP, and was then vacuum dried for 3-4 hours. The overall reaction yield varied from 27-67%. The AgCl nanocubes were then suspended in 5 mL of ethylene glycol. The resulting stock AgCl dispersions were generally used within a week of preparation.

SEM images were collected using a JEOL 7001LVF FE-SEM with an acceleration voltage of 15 kV. TEM images were collected using a JEOL 2000 FX microscope with an acceleration voltage of 200 kV. To prepare SEM samples, a few drops of the purified product (diluted in water) were drop casted onto the Si(111) wafer and air dried. To prepare the TEM samples, TEM grids (copper, coated with holey carbon film, from Ted Pella) were dipped into the reaction solution or purified Ag NWs (diluted in water) and air dried.

XRD patterns were collected on Rigaku DmaxA diffractometer using Cu Kα radiation (λ = 1.541 845 Å) and Materials Data Inc. (MDI) software, and were processed using the JADE software package. To prepare the XRD samples, a few drops of a sample dispersion were drop

casted onto the glass XRD sample holder and dried in the fume hood overnight. The process was repeated until a uniform layer was visible. Refinements of XRD data to quantify phase composition were performed using Powdercell 2.4 freeware.[32]

UV-visible spectra were acquired using a Varian Cary 100 Bio UV-visible spectrophotometer. Samples were prepared by adding 10 drops of the reaction mixture and 3 mL of water into a glass cuvette. Elemental analyses for C, H, and N were conducted by Galbraith Laboratories, Inc. (Knoxville, TN).

2.2.2 Synthesis of silver nanowires (Ag NWs)

The procedure was adapted from a previously reported synthesis.[11] PVP (334 mg, 3.0 mmol) was dissolved in ethylene glycol (20 mL) and refluxed with stirring in an oil bath at 180 ˚C. The surfactant PVP helped stabilize the nanoparticles formed in solution and prevented its agglomeration.[11] The reaction mixture was maintained under these conditions for 5 min, and then varying amounts of NaCl and $AgNO_3$, or alternatively AgCl nanocubes, were added, as described below:

2.2.2.1 High-concentration addition of NaCl and $AgNO_3$. Ethylene glycol solutions of NaCl (1.2 mL, 0.43 M) and $AgNO_3$ (1.2 mL, 0.43 M) were simultaneously injected into the stirring, hot reaction mixture to achieve a final AgCl concentration of 24 mM. The procedure continues in part 2.2.2.4 below.

2.2.2.2 Low-concentration addition of NaCl and $AgNO_3$. Ethylene glycol solutions of NaCl (50 μL, 0.43 M) and $AgNO_3$ (50 μL, 0.43 M) were simultaneously injected into the stirring, hot reaction mixture to achieve a final AgCl concentration of 1.1 mM. The procedure continues in part 2.2.2.4 below.

2.2.2.3 Addition of pre-synthesized AgCl nanocubes. A stock dispersion of AgCl was sonicated for a few seconds prior to use. An aliquot was removed from the dispersion (0.5 mL, 0.2 - 0.4 M) of AgCl) and injected into the stirring, hot reaction mixture to achieve a final AgCl concentration of 4.8 - 9.8 mM. The procedure continues in part 2.2.2.4 below.

2.2.2.4 Growth and purification of Ag NWs. The reaction mixture obtained from part 2.2.2.1-3 above was refluxed for an additional 25 min with stirring. Then a $AgNO_3$ solution (10 mL, 0.12 M) was added dropwise at a rate of 25 mL/h while maintaining reflux and stirring. Silver-gray opalescent swirls of precipitate were observed within 15-20 min of the addition period, indicative of Ag NW formation. At that point, the addition rate was increased to complete addition within 1 min. The mixture was then refluxed for an additional 15 min.

The reaction mixture was allowed to cool to room temperature. H_2O (100 mL) was added to the mixture. Fractions of the mixture (10-12 mL) were successively removed and centrifuged on a bench-top unit. The precipitated Ag NWs were collected and combined, and the yellow supernatant fractions were discarded. The mass yield was recorded, and analyzed as described below.

2.2.2.5 Yield and Characterization of Ag NWs. Elemental analysis of a representative Ag-NW specimen from the synthetic procedures above revealed a negligible amount of residual organics (C, <0.5%; H, <0.5%; N, <0.5%), indicating that the PVP was removed by the work-up procedure (part 2.2.2.4, above). XRD patterns of Ag NWs showed reflections from both Ag and AgCl (Figures A2.1, A2.2), in relative amounts that varied with the synthetic procedure. The XRD data were refined to quantify the Ag and AgCl volume fractions. The refinements produced fitted sum patterns (Figures A2.1, A2.2) and the volume percentages of Ag and AgCl

in the specimens. Three separate refinement runs were performed on each XRD pattern analyzed, and the results were averaged. These values were used with the recorded product masses to provide the percent yields reported in Table 2.1

The residual AgCl in the specimens was removed by the following procedure. A Ag-NW product was redispersed in water (5 mL) and NH_4OH (2 mL, 28.0 – 30.0 w/w %) was added to the dispersion. The dispersion was shaken and then centrifuged. The precipitated Ag NWs were collected and the supernatant was discarded. XRD patterns (Figure A2.3) obtained of the Ag NWs after this wash confirmed the removal of AgCl.

Trials in which the dropwise addition of the $AgNO_3$ solution was incomplete when the formation of Ag NWs was observed (by visualization of gray opalescent swirls) resulted in the formation of a solid lump of byproduct. In some cases this lump was sufficiently large (0.3 - 1.0 cm diameter) to be easily manually separated from the Ag NWs, while in other cases it broke up into smaller pieces and became intermixed with the Ag NWs. Trials in which the dropwise addition of the $AgNO_3$ solution was completed before the Ag NW growth was observed did not produce such a byproduct lump. Elemental analysis of a representative lump revealed small amounts of residual organics (C, 1.36%; H, <0.5%; N, <0.5%). An XRD pattern (Figure A2.4) of the lump showed it to be a mixture of AgCl (80.4 vol %) and Ag (19.6 vol %). As shown in Table 2.1, the trials that did not produce a lump had higher yields of Ag NWs. Additionally, the amount of residual AgCl in the Ag-NW product was lower in reactions that had a separable lump. Trials employing a lower initial NaCl concentration also produced a lower yield of AgCl, and a higher yield of Ag NWs.

2.3 Results

2.3.1 Description of the synthetic process

As in previous studies,[18,20,22,23,25-27] NaCl was used to promote Ag-NW growth in the polyol synthesis. In a typical procedure employing a comparatively large initial concentration of NaCl (24 mM), a solution of PVP in ethylene glycol was heated to 180 °C prior to addition of NaCl. Equimolar quantities of NaCl and $AgNO_3$ were then added to the hot solution, resulting in the instantaneous formation of a white precipitate. XRD patterns (Figure 2.1a, b) obtained from aliquots of the mixture established the precipitate to be AgCl, as has been previously demonstrated.[18,20-22,27]

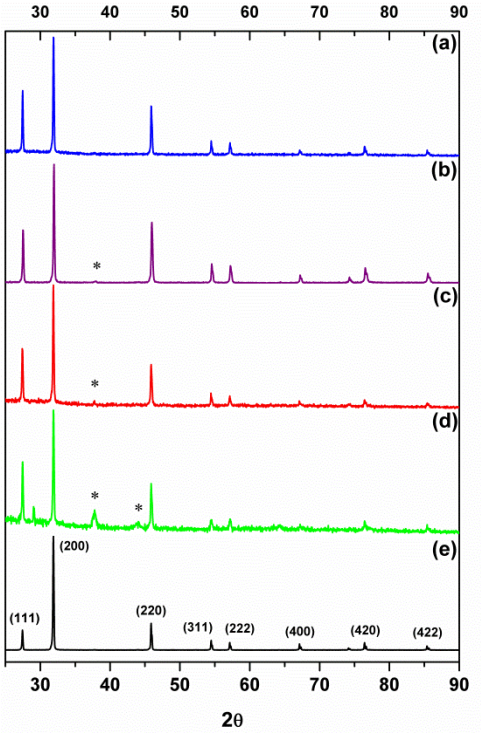

Figure 2.1 XRD patterns of an aliquot taken from reaction with (a) high NaCl concentration 1 min after initial addition of NaCl and $AgNO_3$ (blue), (b) high NaCl concentration 25 min after initial addition of NaCl and $AgNO_3$ (purple), (c) low NaCl concentration 1 min after initial addition of NaCl and $AgNO_3$ (red) and (d) low NaCl concentration 25 min after initial addition of NaCl and $AgNO_3$ (green). (e) XRD pattern of pre-synthesized AgCl nanocubes (black). Asterisks identify reflections from metallic Ag.

The mixture was then stirred at 180 °C for 30 minutes, which was found empirically to maximize the eventual yield of Ag NWs. During this period the color of the mixture turned from white to a creamy yellow, which gradually darkened. XRD patterns of aliquots taken at various times evidenced the formation of small amounts of metallic Ag (Figure 2.1a, b). Spectroscopic monitoring by UV-visible spectroscopy revealed the emergence of the plasmon feature for metallic Ag at a wavelength of 435 nm after 6 min (Figure 2.2), which blue-shifted with time (435 - 402 nm).

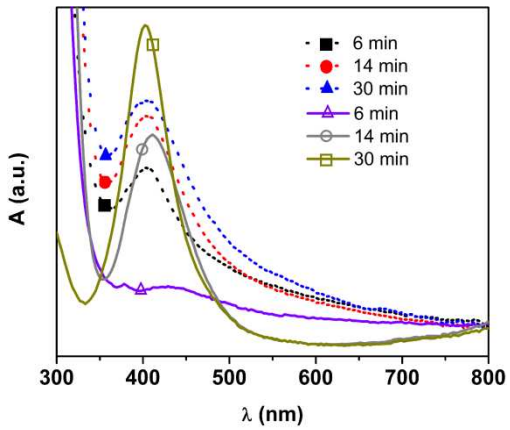

Figure 2.2 UV-visible spectra of aliquots removed from reaction mixtures at various times. The solid curves correspond to a high NaCl concentration experiment, and the dashed curves to a low NaCl concentration experiment.

Dropwise addition of a $AgNO_3$ solution was then initiated. A series of color changes ensued. The mixture became an olive color after about 10 min, and light brown after about 12 min. Silver-gray opalescent swirls appeared in the mixture after about 20 minutes, which indicated the formation of Ag NWs as established by SEM imaging (Figure 2.3b). The NWs were revealed to be pentagonally twinned in higher-magnification images (Figure A2.5), as has been previously reported.[24] The remainder of the $AgNO_3$ solution, if any, was added at a faster rate at this stage.

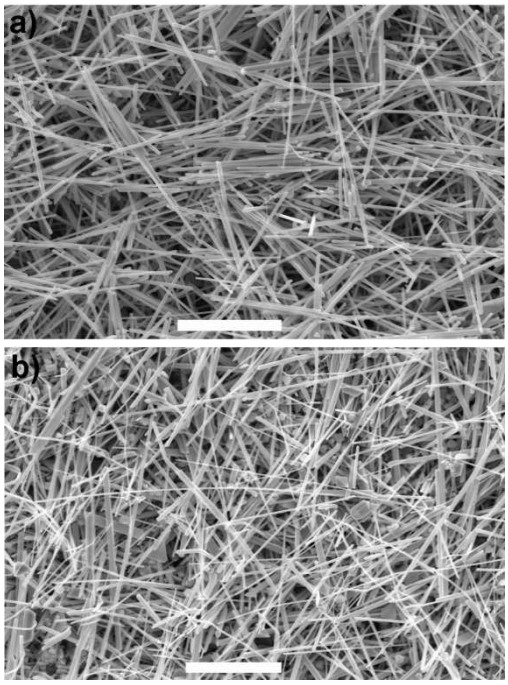

Figure 2.3 SEM images of purified wires synthesized with a) low NaCl concentration, b) high NaCl concentration. The scale bars are 10 μm.

Trials in Ag-NW formation was observed prior to the completion of $AgNO_3$ addition were typically accompanied by the formation of a lump of precipitate that was visually distinct from the dispersion of Ag NWs. Analysis of the lump material showed it to contain a vanishingly small amount of PVP, and to consist of AgCl (61.3 ± 0.7 mol%) intermixed with a smaller amount of metallic Ag (38.7 ± 0.7 mol%; see the Experimental Section). Predictably, the yield of Ag NWs was decreased by this byproduct-lump formation (see text below and Table 2.1).

Table 2.1 Ag and AgCl reaction yields based on AgCl source and concentration, and ethylene glycol purity.

Concentration of AgCl (mM)	% yield Ag[a]	% yield AgCl[a]	Reaction products	Ethylene glycol used
1.1	92.7 ± 0.18	0.82 ± 0.13	Ag NWs (See Figure A2.1)	
24	41.2 ± 0.73	24.2 ± 0.55	Ag NWs and lump intermixed (See Figure A2.2)	Aldrich[c]
0.36[b]	87.9 ± 0.21	0.55 ± 0.16	Ag NWs and separate lump	
1.1	79.8 ± 0.23	0.82 ± 0.17	Ag NWs and separate lump	J. T Baker[d]
24	56.9 ± 0.09	4.29 ± 0.06	Ag NWs and separate lump	

[a]The reaction yields of the products before washing with NH_4OH. [b]Using pre-synthesized AgCl nanocubes. [c]Ethylene glycol from Aldrich had no certificate of analysis. [d]The impurities listed in the ethylene glycol from J. T. Baker are as follows: Cl; max. 5 ppm, Fe; max. 0.200 ppm.

The procedure was also conducted using a smaller initial concentration of NaCl (1.1 mM). In this case a white AgCl precipitate was not evident upon addition of equimolar quantities of NaCl and $AgNO_3$ to the PVP solution at 180 °C. Instead, a clear yellow solution formed. To establish the presence or absence of AgCl, the reaction was discontinued in two trials during the 30-min stirring period. After the reaction mixtures cooled, acetone was added, resulting in dark precipitates. XRD patterns of these precipitates (Figure 2.1c, d) established the presence of AgCl as the dominant phase, with smaller amounts of metallic Ag. The reaction, when continued as described above for the high-NaCl-concentration procedure, underwent a

similar series of color changes upon further addition of $AgNO_3$. SEM images (Figure 2.3a) established the formation of Ag NWs as above.

Elemental analysis of a representative Ag-NW product showed that it contained no detectable PVP, establishing its removal in the work-up procedure. XRD analyses revealed that the Ag NWs contained varying amounts of residual AgCl, which scaled with the initial concentration of NaCl and the successful separation of the byproduct lump (if any). Syntheses employing a low initial NaCl concentration gave Ag-NW product yields of up to 93%, with a AgCl contamination of < 1% (Table 2.1). In contrast, syntheses employing a high initial NaCl concentration gave lower Ag-NW product yields of 40-60%, with a AgCl contamination as high as 24% (Table 2.1). Lump formation was much less common in trials conducted at low initial NaCl concentration. The residual AgCl was removed by washing the Ag-NW product with aqueous NH_4OH, as confirmed by XRD (Figure A2.3). An SEM image of washed material confirmed that the Ag NWs were unaffected (Figure A2.6).

2.3.2 Reaction monitoring by SEM and TEM

An aliquot from a reaction mixture was taken during the 30-min stirring period after addition of equimolar quantities of NaCl and $AgNO_3$ (high-concentration trial). SEM images revealed faceted nanocrystals having cuboidal, cuboctahedral, and related morphologies (Figure 2.4a). We surmised these nanocrystals to be composed of AgCl, which was the major phase found by XRD (Figure 2.1a, b). SEM images obtained from aliquots from a low-concentration trial at the same reaction stage also contained cuboidal and cuboctahedral nanocrystals (Figure 2.4b), although the size distribution was shifted towards smaller sizes.

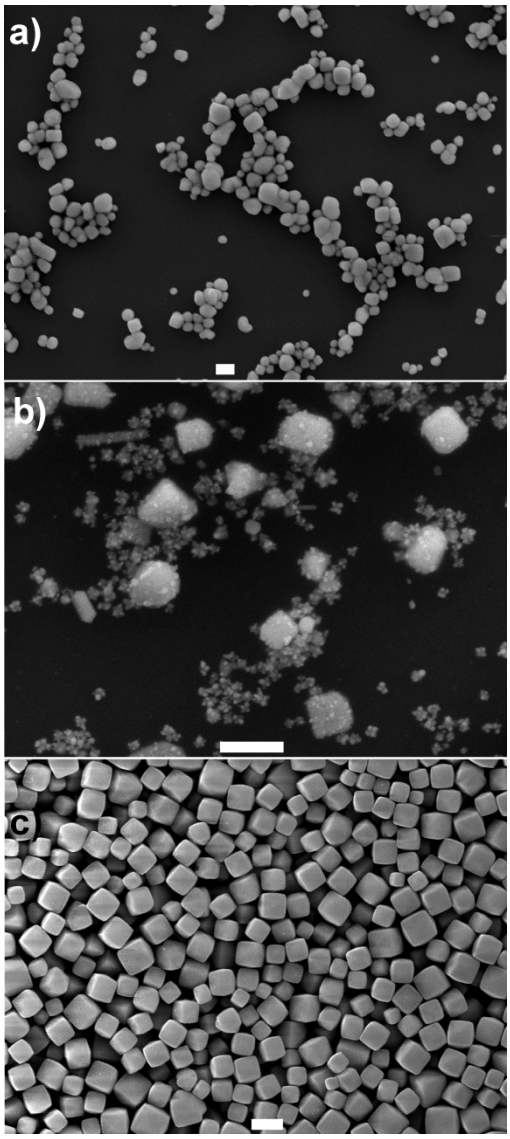

Figure 2.4 SEM images of a) an aliquot removed from a high NaCl concentration reaction, b) an aliquot removed from a low NaCl concentration reaction, and c) independently synthesized AgCl nanocubes. The scale bars are 1 μm.

SEM images of the nanocrystals harvested in situ were compared to those of independently synthesized AgCl nanocrystals[31] (XRD pattern in Figure 2.1e) to provide further verification of their identity. As shown in Figure 2.4c, the independently synthesized AgCl nanocrystals exhibited closely similar morphologies. Elemental analyses by energy-dispersive X-ray spectroscopy (EDS) found both Ag and Cl, although the ratios were unreliable due to the

instability of the nanocrystals under the electron beam. Under irradiation, small nodules of metallic Ag were observed to form on the AgCl nanocrystals, as the Ag:Cl ratio continued to increase with irradiation time (Figure A2.7). This instability was further visualized by comparing regions in the images that had been rastered by the electron beam with regions that were minimally exposed. The exposed regions were visibly darker due to metallic-Ag formation (Figure A2.8).[31]

TEM imaging of the independently synthesized AgCl nanocrystals gave similar results. Electron-beam damage of the nanocubes ensued immediately upon beam focusing, resulting in metallic-Ag nanoparticle formation on the cube surfaces (Figure 2.5a). Thus, images of pristine AgCl nanocubes were difficult to obtain (as in Figure 2.4c). In certain specimens, synthesized at lower HCl concentrations,[31] filaments of metallic Ag were found to emanate from the AgCl cubes upon electron-beam exposure (Figure 2.5b), suggesting the initiation of NW growth. One can imagine such filaments developing into Ag NWs under reaction conditions (see below).

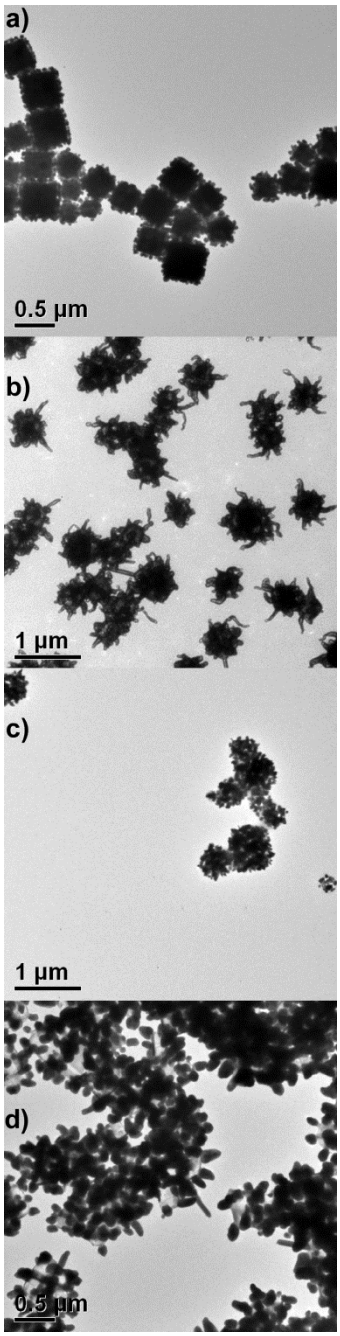

Figure 2.5 TEM images of nodules and filaments of Ag growing from AgCl cubes upon e-beam exposure; a) and b) independently synthesized AgCl cubes, c) and d) AgCl nanocubes from reaction mixtures employing added NaCl.

AgCl nanocubes harvested from a Ag-NW synthesis during the 30-minute stirring period were also examined by TEM (Figure 2.5c, d). The images of the nanocubes resembled those of

the independently synthesized AgCl (Figure 2.5a, b), exhibiting Ag particles and filaments on the cube surfaces. As above, the majority of the Ag surface decoration formed upon beam exposure in the TEM. The XRD and UV-visible-spectroscopic monitoring experiments described above established some Ag formation during the 30-minute stirring period. However, the resulting Ag nanostructures were obscured by the rapid Ag formation under the electron beam, and thus could not be imaged due to the extreme beam sensitivity of the AgCl nanocubes. Although direct evidence was therefore lacking, we presumed that the Ag initially formed under the reaction conditions was deposited on the surfaces of the AgCl nanocubes.

Another aliquot was taken from a low-NaCl-concentration Ag NW synthesis during the $AgNO_3$ dropwise-addition period, prior to the visual observation of silver-gray opalescent swirls indicative of extensive NW growth. A TEM image taken of the aliquot is shown in Figure 2.6. The image reveals comparatively large Ag nodules on the faces and vertices of the AgCl nanocubes. In Figure 2.6, the AgCl nanocubes appear to be colorless with gray patches, whereas the Ag nodules appear to be considerably darker. We have inserted cartoon representations into the Figure-2.6 image to assist the visualization of these nanostructures. As above, the majority of the Ag-nodule formation occurred in the microscope under e-beam exposure. However, the pattern of Ag-nodule decoration on the cubes presumably resulted from an underlying pattern of pre-existing Ag nuclei present on the cubes prior to beam exposure.

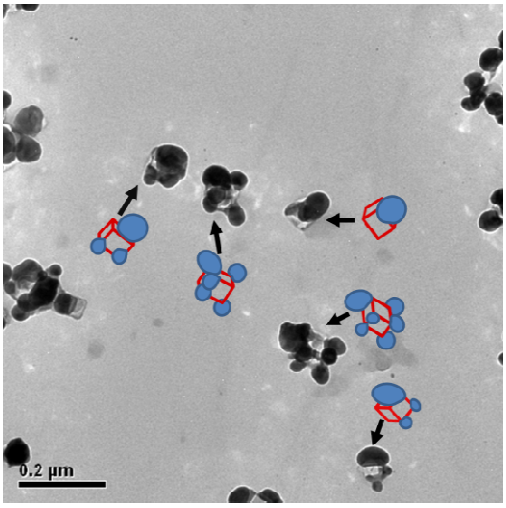

Figure 2.6 A TEM image of AgCl nanocubes generated in a reaction mixture employing added NaCl. The dark nodules decorating the nanocubes are Ag nanoparticles. In the inset cartoons, the AgCl nanocubes are depicted in red and the Ag nanoparticles in blue.

A related aliquot from a low-NaCl-concentration Ag NW synthesis was examined by SEM, prior to the visual observation of silver-gray opalescent swirls indicative of extensive NW growth (Figure 2.7). Small AgCl cubes with Ag-nodule decoration like those in Figure-2.6 TEM images were observed in the Figure-2.7 SEM images as well. Additionally, the Figure-2.7 SEM images clearly showed that short segments of Ag NWs were beginning to form. Careful inspection revealed that these NW segments were generally adhering to a AgCl nanocuboid, to which was also attached ≥ 4 Ag nanoparticles. Several such nanostructures are identified by arrows in Figure 2.7, and one is rendered in cartoon form to aid in visualization. The results strongly suggested that Ag NW growth resulted from elongation of a Ag nodule formed on the AgCl nanocube at the earlier stage represented by the Ag-nodule-decorated nanocubes evident in both Figures 2.6 and 2.7. Generally, only a single Ag NW was found emanating from a nanocube cluster.

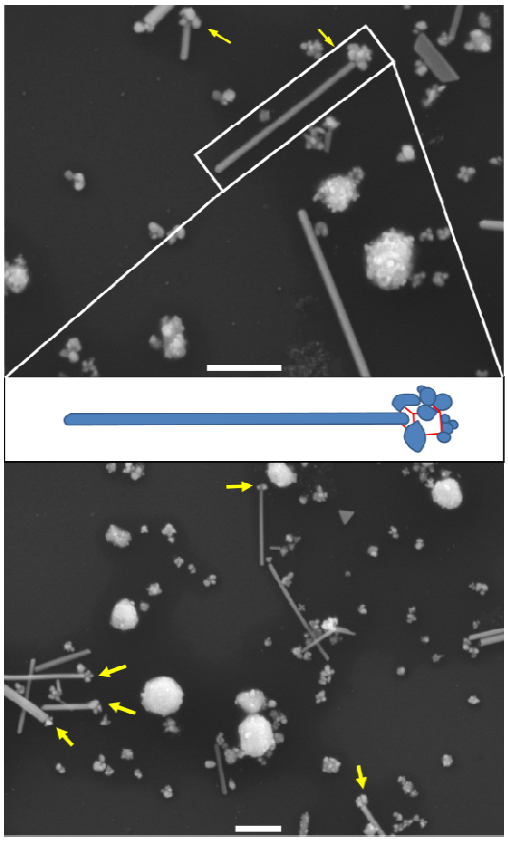

Figure 2.7 SEM images taken of an aliquot from a reaction mixture employing added NaCl (low-concentration trial). The aliquot was removed 5 min after the start of dropwise addition of $AgNO_3$ solution. The arrows mark Ag NWs emanating from AgCl nanocuboids (see text). One such nanostructure is depicted in cartoon form. The scale bars are 1 μm.

A related aliquot was taken from a high-NaCl-concentration Ag NW synthesis, 10 min after the stirring period, during the dropwise $AgNO_3$ addition, and prior to extensive NW growth. SEM images (Figure 2.8) revealed aggregated piles of large Ag nanoparticles, which in some cases appeared to be remnants of formerly cubic structures. Such pseudo-cubic piles apparently resulted from the reduction of large AgCl cubes to Ag particles. One or more Ag NWs were infrequently found to emanate from these nanoparticle piles, in a manner reminiscent of the clearer results in Figure 2.7.

Small AgCl nanocubes like those evident in Figure 2.7 were absent from images like those in Figure 2.8. Moreover, a reexamination of Figure 2.7 showed that the smaller AgCl

nanocubes were more likely to nucleate Ag NWs than were the larger AgCl nanocubes also evident in Figure 2.7. The results were consistent with the final NW images in Figure 2.3, which revealed that the low-NaCl-concentration synthesis was more selective for NW growth (Figure 2.3a). The high-NaCl-concentration synthesis (Figure 2.3b) contained a larger Ag nanoparticle fraction and a broader diameter distribution for the Ag NWs. Thus, the small AgCl nanocubes produced at low NaCl concentration were more-effective nucleating agents for Ag NW growth.

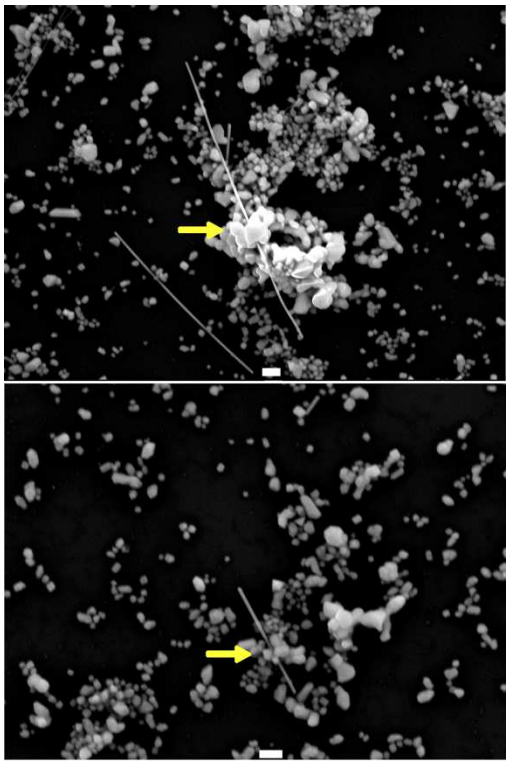

Figure 2.8 SEM images taken of an aliquot from a reaction mixture employing added NaCl (high-concentration trial). The aliquot was removed 10 min after the start of dropwise addition of $AgNO_3$ solution. The scale bars are 1 μm. The arrows identify piles of Ag nanoparticles that may be remnants of large AgCl nanocubes.

2.3.3 Ag NW growth from pre-synthesized AgCl nanocubes

The results above suggested that the Ag NWs were nucleated by the AgCl nanocubes, or, more precisely, that they were grown from the Ag nanoparticles themselves heterogeneously nucleated upon the AgCl nanocubes. If so, then the direct addition of pre-synthesized AgCl nanocubes should be sufficient to induce NW growth, without the NaCl additive. Synthetic trials were conducted as above, with the addition of dispersions of pre-synthesized AgCl nanocubes (Figure 2.4c) in place of the initial, equimolar quantities of $AgNO_3$ and NaCl. Color changes and other experimental observations paralleled those described above.

An SEM image of an aliquot taken 23 minutes after the start of dropwise $AgNO_3$ addition is shown in Figure 2.9a. Ag NWs were observed to have grown from AgCl nanocube surfaces. An SEM image of the purified Ag NW product is shown in Figure 2.9b. The results established that AgCl nanocubes were necessary and sufficient for the growth of Ag NWs.

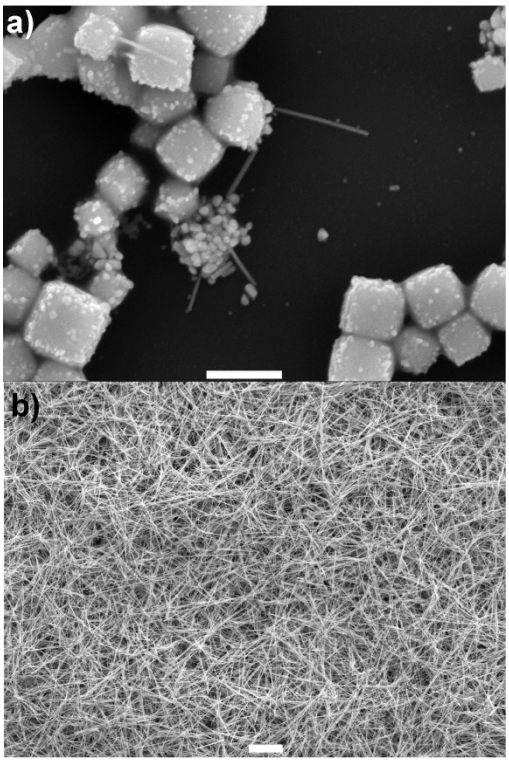

Figure 2.9 (a) SEM image taken of an aliquot from a reaction mixture employing pre-synthesized AgCl nanocubes. The aliquot was removed 23 min after the start of dropwise addition of $AgNO_3$ solution. The scale bar is 1 μm. (b) SEM image of purified Ag NWs obtained from a synthesis employing pre-synthesized AgCl nanocubes. The scale bar is 10 μm.

The yields of the Ag NWs grown with the pre-synthesized AgCl nanocubes approached 90%, and were thus comparable to the best yields obtained from low-NaCl-concentration trials (Table 2.1). The NWs were obtained with minimal AgCl contamination (Table 2.1). The quality of the product in selectivity for NW formation and diameter distribution (Figure 2.9b) was equal to or surpassed that achieved in the low-concentration-NaCl synthesis (Figure 2.3a).

2.3.4 Supporting evidence for heterogeneous nucleation

If heterogeneous nucleation on AgCl nanocubes was the primary nucleation mechanism for Ag NWs, then, with a constant amount of $AgNO_3$ additive (after AgCl formation), the length of the Ag NWs should anticorrelate with the number of AgCl nanocubes present. Smaller numbers of

AgCl nanocubes should on average produce longer wires. If one assumes that high initial AgCl concentrations produce larger numbers of AgCl nanocubes than do low initial AgCl concentrations, then the low NaCl-concentration trials should produce longer wires than do the high NaCl-concentration trials. This hypothesis was experimentally tested.

The Ag NW length distributions from representative high (blue) and low (red) NaCl-concentration trials are plotted in Figure 2.10. These distributions were constructed using random length measurements obtained from SEM images. The measurements were collected from specimens having low NW-coverage densities such that individual NWs were readily discerned in the images. The mean NW length from the high-concentration trial was 2.2 μm with a standard deviation in the distribution of 1.3 μm, or 60% of the mean length. The mean length from the low-concentration trial was 11.4 μm with a standard deviation in the distribution of 5.7 μm, or 50% of the mean length. The low-concentration trial produced markedly longer mean Ag NW lengths, consistent with expectation for a primary heterogeneous-nucleation mechanism.

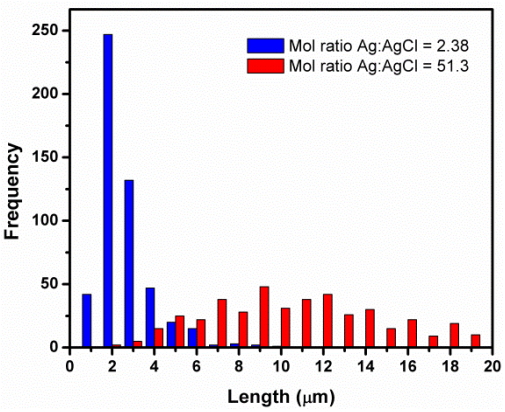

Figure 2.10. A histogram showing the dependence of Ag-NW length on the mole ratio of Ag to AgCl in the reaction mixture. The mole ratio of 2.38 corresponds to a high NaCl-concentration reaction and the mole ratio of 51.3 corresponds to a low NaCl-concentration reaction. The mean lengths were 2.2 μm ± 60% and 11.4 μm ± 50%, respectively.

2.3.5 Control experiments

Previous studies of the polyol synthesis of Ag NWs established that halide additives such as NaCl were essential to the selective formation of NWs rather than other Ag nanoparticle morphologies.[18,22] To confirm the necessity of added chloride (as NaCl) under our conditions, we conducted a control experiment (using Aldrich ethylene glycol) in which NaCl was omitted, but our other reaction parameters were unchanged. An SEM image of the resulting product established that selectivity for NW formation was lost (Figure A2.9a). Instead, a complex mixture of nanoparticle morphologies was observed with a very small proportion of Ag NWs, which were comparatively short. Thus, NaCl addition was shown to be essential to NW selectivity under our conditions as well.

A second control experiment was conducted to examine the role of the second (dropwise) $AgNO_3$ addition. As detailed above, $AgNO_3$ was added in two fractions in our procedure. The initial addition with NaCl was to promote AgCl-nanocube formation, and the second addition was to promote Ag NW growth. However, one may note that AgCl contains Ag+, and was therefore a potentially sufficient source to support NW growth, without the second addition of $AgNO_3$. A synthetic trial in which this second addition was omitted but our other reaction parameters were maintained (for high NaCl concentration) failed to produce Ag NWs (Figure A2.9b). The product contained a large fraction of AgCl nanocubes intermixed with various Ag-nanoparticle morphologies. The result established that the primary source of Ag^+ to support NW growth was the $AgNO_3$ added dropwise in the second fraction,[11] after AgCl-nanocube formation was complete.

Another control experiment demonstrated the importance of the 30-min stirring period after *in-situ* generation of the AgCl nanocubes. As described above, the formation of small amounts of metallic Ag was observed during this period, as determined by XRD and absorption spectroscopy (Figures 2.1 and 2.2). We surmised that this Ag formed upon the surfaces of the AgCl nanocubes (see above), providing nucleation sites for subsequent NW growth. A trial in which the 30-min stirring period was omitted gave a mixture of Ag-nanoparticle morphologies without selectivity for NW growth (Figure A2.9c). The result suggested that the AgCl nanocubes were activated for NW growth by surface-Ag formation during the stirring period.

A final set of control experiments was conducted using high-purity ethylene glycol ($\leq$ 5 ppm Cl, $\leq$ 0.200 ppm Fe) from J. T. Baker for Ag NW growth. The reaction yields were similar to those from syntheses employing Aldrich ethylene glycol (Table 2.1). SEM images (Figure A2.10a, b) of the NWs showed comparable Ag-NW quality and selectivity to NWs grown in Aldrich ethylene glycol. Thus, our synthetic results were not significantly influenced by impurities that may have been present in the Aldrich ethylene glycol.

2.4 Discussion

Four observations strongly indicate that the role of the NaCl additive is to generate AgCl nanocubes, which serve as heterogeneous nucleants for Ag NW growth. (1) Synthetic trials lacking a chloride additive, and therefore AgCl nanocubes, failed to give Ag NWs, producing Ag nanoparticles having other morphologies instead.[18,22] (2) AgCl nanocubes generated independently and added to the syntheses were active for nucleating Ag NWs, functioning in the same manner as the AgCl nanocubes generated *in situ* by NaCl addition. (3) Images of Ag NWs nucleated on and growing from AgCl nanocubes were obtained. (4) The lengths of the Ag NWs

were anti-correlated with the quantity and presumed number density of AgCl nanocubes, as expected for a heterogeneous-nucleation mechanism. The heterogeneous-nucleation and growth process elucidated here is summarized in Scheme 2.1.

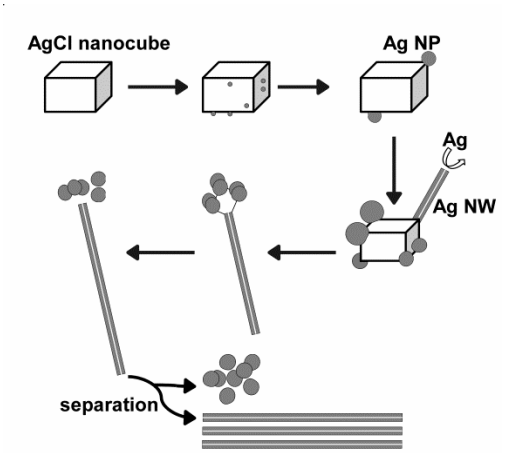

Scheme 2.1. Depiction of the heterogeneous nucleation and growth pathway for Ag NWs.

The Scheme-2.1 pathway bears close similarity to the photographic process employing silver-halide emulsions.[33,34] When silver-halide crystallites in the emulsions are exposed to light, mobile Ag^+ ions in the lattice are reduced by photogenerated electrons. Small Ag_n clusters are formed on the crystallite surfaces, which constitute the (invisible) latent image. At the same time, the photogenerated holes convert halide ions to dihalogen. The latent image is developed by treating the exposed emulsion to a reducing agent. The Ag_n clusters catalyze the complete reduction of the exposed AgX crystallites to metallic Ag. The critical, developable cluster size is believed to be Ag_4, such that the unexposed AgX crystallites are not reduced in development, and remain unreacted. The resulting distribution of metallic Ag particles within the AgX emulsion forms the photographic image.

In the present work, addition of NaCl and $AgNO_3$ to the polymer solution results in the immediate formation of AgCl nanocubes. These are generated in hot ethylene glycol, which is the reductant, and small Ag_n clusters and nanoparticles are formed on the nanocube surfaces during the subsequent stirring period (Scheme 2.1). These clusters and nanoparticles may be "developed" by exposure to an electron beam in a microscope, or by continued reduction under the reaction conditions. Several large Ag nanoparticles typically form on each AgCl nanocube. Some of these Ag nanoparticles become pentagonally twinned. Such twinned nanoparticles were previously shown to grow anisotropically into pentagonally twinned NWs by addition of Ag to the remote tip.[24] Although both the added $AgNO_3$ and the AgCl nanocubes are sources of Ag^+ to feed the reduction process, the second, drop-wise addition of $AgNO_3$ is primarily responsible for NW growth. Even so, the AgCl nanocubes become degraded and partially consumed by reduction, eventually releasing the attached Ag NWs and nanoparticles. The NWs and nanoparticles are separated in the work-up procedure.

2.5 Conclusions

In summary, the role of the NaCl additive, and by analogy other alkali halide additives that have also been employed in polyol Ag NW syntheses, is to generate heterogeneous nucleants in the form of Ag-halide nanocubes. The results reported here establish that the smaller AgCl nanocubes are more-potent heterogeneous nucleants that afford higher selectivity for Ag NW growth and narrower NW diameter distributions. Consequently, improved synthetic control might be achieved by the use of small, presynthesized AgCl nanocubes rather than those generated *in situ* from chloride additives. Efforts are currently underway in our laboratory to determine which reaction parameters may be varied to control Ag NW mean diameter and length.

2.6 References

1. Wiley, B. J.; Im, S. H.; Li, Z. –Y.; McLellan, J.; Siekkinen, A.; Xia, Y. Maneuvering the Surface Plasmon Resonance of Silver Nanostructures through Shape-Controlled Synthesis. *J. Phys. Chem. B* **2006**, *110*, 15666-15675.

2. Kelly, K. L.; Coronado, E.; Zhao, L. L.; Schatz, G. C. The Optical Properties of Metal Nanoparticles: The Influence of Size, Shape and Dielectric Environment. *J. Phys. Chem. B* **2003**, *107*, 668-677.

3. Amendola, V.; Bakr, O. M.; Stellacci, F. A Study of the Surface Plasmon Resonance of Silver Nanoparticles by the Discrete Dipole Approximation Method: Effect of Shape, Size, Structure and Assembly. *Plasmonics* **2010**, *5*, 85-97.

4. Zou, K.; Zhang, X. H.; Duan, X. F.; Meng, X. M.; Wu, S. K. Seed-Mediated Synthesis of Silver Nanostructures and Polymer/Silver Nanocables by UV Irradiation. *J. Cryst. Growth* **2004**, *273*, 285-291.

5. Sun, J.; Zhang, J.; Liu, W.; Liu, S.; Sun, H.; Jiang, K.; Li, Q.; Guo, J. Shape Controlled Synthesis of Silver Nanostructures. *Nanotechnology* **2005**, *16*, 2412-2414.

6. Wiley, B.; Sun, Y.; Mayers, B.; Xia, Y. Shape Controlled Synthesis of Metal Nanostructures: The Case of Silver. *Chem.—Eur. J.* **2005**, *11*, 454-463.

7. Wiley, B.; Sun, Y.; Xia, Y. Synthesis of Silver Nanostructures with Controlled Shapes and Properties. *Acc. Chem. Res.* **2007**, *40*, 1067-1076.

8. Samanta, S.; Pyne, S.; Sarkar, P.; Sahoo, G. P.; Bar, H.; Bhui, D. K.; Misra, A. Synthesis of Silver Nanostructures of Varying Morphologies through Seed Mediated Growth Approach. *J. Mol. Liq.* **2010**, *153*, 170-173.

9. Chen, D.; Qiao, X.; Chen, J. Morphology-Controlled Synthesis of Silver Nanostructures *via* a Solvothermal Method. *J. Mater.Sci.:Mater.Electron.* **2011**, *22*, 1335-1339.

10. Sun, Y.; Xia, Y. Large-Scale Synthesis of Uniform Silver Nanowires through a Soft, Self-Seeding, Polyol Process. *Adv. Mater*. **2002**, *14*, 833-837.

11. Sun, Y.; Yin, Y.; Mayers, B. T.; Herricks, T.; Xia, Y. Uniform Silver Nanowires Synthesis by Reducing $AgNO_3$ with Ethylene Glycol in the Presence of Seeds and Poly(Vinyl Pyrrolidone). *Chem. Mater*. **2002**, *14*, 4736-4745.

12. Gao, Y.; Jiang , P.; Liu, D. F.; Yuan, H. J.; Yan, X. Q.; Zhou, Z. P.; Wang, J. X.; Song, L.; Liu, L. F.; Zhou, W. Y. *et al.* Synthesis, Characterization and Self-Assembly of Silver Nanowires. *Chem. Phys. Lett.* **2003**, *380*, 146-149.

13. Tsuji, M.; Nishizawa, Y.; Hashimoto, M.; Tsuji, T. Syntheses of Silver Nanofilms, Nanorods, and Nanowires by a Microwave-Polyol Method in the Presence of Pt Seeds and Polyvinylpyrrolidone. *Chem. Lett.* **2004**, *33*, 370-371.

14. Wiley, B.; Sun, Y.; Xia, Y. Polyol Synthesis of Silver Nanostructures: Control of Product Morphology with Fe(II) or Fe(III) Species. *Langmuir* **2005**, *21*, 8077-8088.

15. Gao, Y.; Jiang, P.; Song, L.; Liu, L.; Yan, X.; Zhou, Z.; Liu, D.; Wang, J.; Yuan, H.; Zhang, Z. *et al.* Growth Mechanism of Silver Nanowires Synthesized by

Polyvinylpyrrolidone-Assisted Polyol Reduction. *J. Phys. D: Appl. Phys*. **2005**, *38*, 1061-1067.

16. Chen, C.; Wang, L.; Jiang, G.; Yang, Q.; Wang, J.; Yu, H.; Chen, T.; Wang, C.; Chen, X. The Influence of Seeding Conditions and Shielding Gas Atmosphere on the Synthesis of Silver Nanowires through the Polyol Process. *Nanotechnology* **2006**, *17*, 466-474.

17. Chen, C.; Wang, L.; Jiang, G.; Zhou, J.; Chen, X.; Yu, H.; Yang, Q. Study on the Synthesis of Silver Nanowires with Adjustable Diameters through the Polyol Process. *Nanotechnology* **2006**, *17*, 3933-3938.

18. Tsuji, M.; Matsumoto, K.; Jiang, P.; Matsuo, R.; Tang, X.-L.; Kamarudin, K. S. N. Roles of Pt Seeds and Chloride Anions in the Preparation of Silver Nanorods and Nanowires by Microwave Polyol Method. *Colloids Surf., A* **2008**, *316*, 266-277.

19. Korte, K. E.; Skrabalak, S. E.; Xia, Y. Rapid Synthesis of Silver Nanowires through a CuCl- $CuCl_2$ Mediated Polyol Process. *J. Mater. Chem*. **2008**, *18*, 437-441.

20. Gou, L.; Chipara, M.; Zaleski, J. M. Convenient Rapid Synthesis of Silver Nanowires. *Chem. Mater*. **2007**, *19*, 1755-1760.

21. Li, Z. C.; Shang, T. M.; Zhou, Q. F.; Feng, K. Sodium Chloride Assisted Synthesis of Silver Nanowires. *Micro & Nano Letters* **2011**, *6*, 90-93.

22. Coskun, S.; Aksoy, B.; Unalan, H. E. Polyol Synthesis of Silver Nanowires: An Extensive Parametric Study. *Cryst. Growth Des.* **2011**, *11*, 4963-4969.

23. Lin, H.; Ohta, T.; Paul, A.; Hutchison, J. A.; Demid, K.; Lebedev, O.; Tendeloo, G. V.; Hofkens, J.; Uji-i, H. Light-Assisted Nucleation of Silver Nanowires During Polyol Synthesis. *J. Photochem. Photobiol., A* **2011**, *221*, 220–223

24. Sun, Y.; Mayers, B.; Herricks, T.; Xia, Y. Polyol Synthesis of Uniform Silver Nanowires: A Plausible Growth Mechanism and the Supporting Evidence. *Nano Lett.* **2003**, *3*, 955-960.

25. Wiley, B.; Herricks, T.; Sun, Y.; Xia, Y. Polyol Synthesis of Silver Nanoparticles: Use of Chloride and Oxygen to Promote the Formation of Single-Crystal, Truncated Cubes and Tetrahedrons. *Nano Lett.* **2004**, *4*, 1733-1739.

26. Wiley, B.; Sun, Y.; Xia, Y. Synthesis of Silver Nanostructures with Controlled Shapes and Properties. *Acc. Chem. Res.* **2007**, *40*, 1067-1076.

27. Zhang, W. C.; Wu, X. L.; Chen, H. T.; Gao, Y. J.; Zhu, J.; Huang, G. S.; Chu, P. K. Self-Organized Formation of Silver Nanowires, Nanocubes and Bipyramids *via* a Solvothermal Method. *Acta Mater.* **2008**, *56*, 2508-2513.

28. Hu, L.; Kim, H. S.; Lee, J.-Y.; Peumans, P.; Cui, Y. Scalable Coating and Properties of Transparent, Flexible, Silver Nanowire Electrodes. *ACS Nano*. **2010**, *4*, 2955-2963.

29. Liu, S.; Yue, J.; Gedanken, A. Synthesis of Long Silver Nanowires from AgBr Nanocrystals. *Adv. Mater*. **2001**, *13*, 656-659.

30. Im, S. H.; Lee, Y. T.; Wiley, B.; Xia, Y. Large Scale Synthesis of Silver Nanocubes: The Role of HCl in Promoting Cube Perfection and Monodispersity. *Angew. Chem., Int. Ed*. **2005**, *44*, 2154-2157.

31. Kim, S.; Chung, H.; Kwon, J. H.; Yoon, H. G.; Kim, W. Facile Synthesis of Silver Chloride Nanocubes and their Derivatives. *Bull. Korean Chem. Soc.* **2010**, *31*, 2918-2922.

32. Kraus, W.; & Nolze, G.; **1996**. *POWDER CELL* - A Program for the Representation and Manipulation of Crystal Structures and Calculation of the Resulting X-Ray Powder Patterns. *J. Appl. Crystallogr*. *29*, 301-303.

33. James, T. H. The Theory of the Photographic Process. *Mechanism of Formation of the Latent Image*; Hamilton, J. F., Eds; Macmillan Publishing Co. Inc.: New York, 1977; pp 105-133.

34. Hamilton, J. F. The Silver Halide Photographic Process. *Advances in Physics* **1988**, *37*, 359-441.

Chapter 3

Polyol Synthesis of Silver Nanowires by Heterogeneous Nucleation; Mechanistic Aspects Influencing Nanowire Diameter and Length

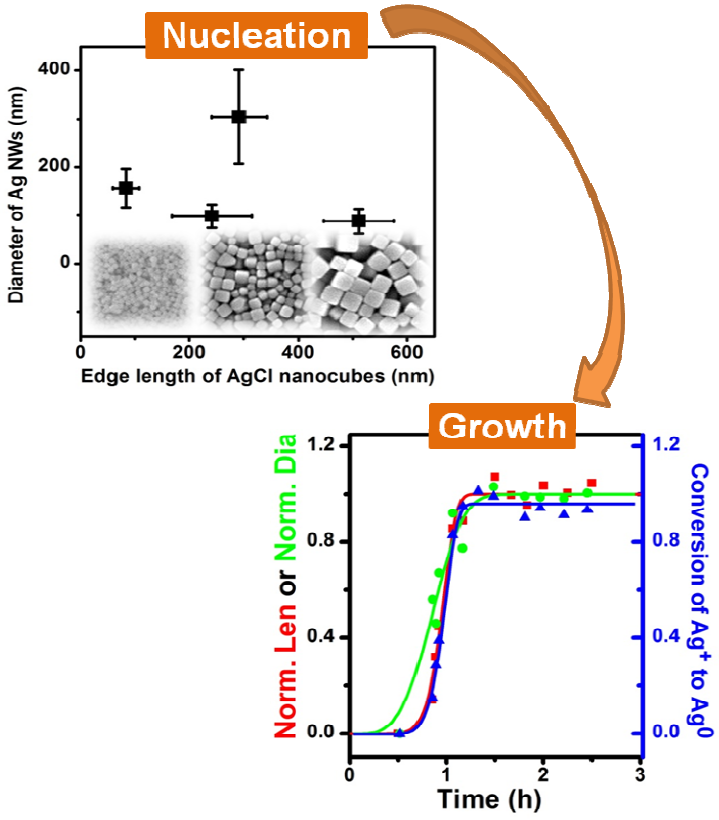

3.1 Introduction

Silver nanowires (Ag NWs) grown by the polyol method[1] employing NaCl as an additive are heterogeneously nucleated on AgCl nanocubes formed *in situ*.[2] We show herein that the diameters of the Ag NWs are not determined by the nucleation event, and are independent of the size of the AgCl-nanocube nucleants. Rather, the NW diameters, lengths, and aspect ratios increase continuously over the entire time scale of the Ag^+ reduction. Our results support a surface-catalyzed reduction process occurring on both the (111) tip facets and the (100) side facets of the growing Ag NWs, which is reduction-rate limited.

Polyol syntheses of Ag NWs require specific additives, such as NaCl,[3,4] to achieve high yields and selectivities. In a recent study,[2] we demonstrated that the role of the NaCl additive is to generate AgCl nanocubes, upon which the Ag^+ reduction reaction is initiated (Scheme 1) and metallic Ag is nucleated. The AgCl nanocubes become decorated by Ag nanoparticles, some of which are pentagonally twinned and grow into NWs (see Figure B3.1). The nanocubes are largely degraded over the course of the growth process, releasing the Ag nanoparticles and NWs, which are separated during the work up. Few NWs are obtained in the absence of AgCl nanocubes.

Our discovery of this heterogeneous-nucleation mechanism suggested the possibility of a relationship between the size of the heterogeneous nucleant and the diameter of the Ag NW nucleated from it. We note that such a relationship exists in other catalyzed NW-growth methods. In the vapor-liquid-solid (VLS)[5-7] and solution-liquid-solid (SLS) mechanisms,[8] NW diameters scale with the diameters of the metallic nanoparticles (droplets) catalyzing growth.

Here, we studied the growth of Ag NWs from AgCl nanocubes over a range of nanocube edge lengths, finding no relationship between edge length and NW diameter.

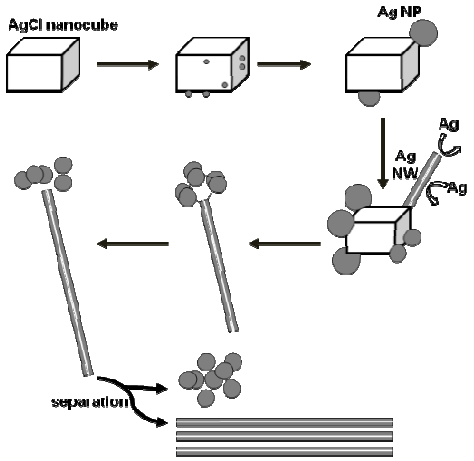

Scheme 2.1 Heterogeneous nucleation and growth pathway for Ag NWs. The present study shows that Ag deposition occurs on both the tip and side-wall NW surfaces.

We next sought to understand how the diameters, lengths, and aspect ratios of the Ag NWs evolved over the growth process. We report here the kinetics of the Ag^+ reduction process, and the growth of the NWs in diameter, length, and aspect ratio as a function of reaction temperature. Interestingly, the kinetic profiles of the reduction, diameter increase, length increase, and aspect-ratio increase parallel one another closely, showing that the growth in all three NW-size parameters corresponds to the time scale of the reduction process.

That is, Ag NW growth is coupled to the reduction reaction, which excludes significant contributions by nanoparticle aggregation[9,10] or Ostwald ripening[11] to the growth mechanism under the conditions we employed. Moreover, the concomitant growth in diameter and length indicates that Ag deposition occurs on *all* NW surfaces, not just at the tip, strongly suggesting a rate-limiting surface-catalyzed Ag^+ reduction reaction. Consequently, Ag NW diameters are not

fixed upon nucleation or at any later time until the conclusion of the Ag^{+} reduction, and are thus not readily controlled in this polyol synthesis.

3.2 Experimental Section

3.2.1 General Methods. All syntheses were conducted under ambient conditions. Ethylene glycol (>99.0 %, J. T. Baker), $AgNO_3$ (99+%, Aldrich), polyvinylpyrrolidone (PVP, MW ≈ 55,000, Aldrich), glycolaldehyde dimer (Aldrich), concentrated nitric acid (70% reagent grade, Aldrich), concentrated hydrochloric acid (37% reagent grade, Aldrich), and acetone (reagent grade, Aldrich) were used as received without further purification. Si(111) wafers were purchased from Aldrich. Deionized water was used in all procedures.

SEM images were collected using a JEOL 7001LVF FE-SEM with an acceleration voltage of 15 kV. To prepare SEM samples, a few drops of the purified product (diluted in water) were drop casted onto the Si(111) wafer and air dried. Image analysis was conducted using ImageJ freeware (http://rsb.info.nih.gov/ij/),[12] for constructing diameter and length distributions. Approximately 200 measurements were made to obtain each data point in mean edge lengths of AgCl nanocubes (for Table 3.1 and Figure 3.1) and lengths and diameters of Ag NWs (for Figures 3.2, 3.6, 3.7 and 3.8).

^{1}H NMR spectra were acquired on a 300-MHz Varian INOVA-300 spectrometer.

3.2.2 AgCl Nanocube Synthesis

The procedure was adapted from a previously published synthesis.[13] PVP (416 mg, 3.75 mmol) and $AgNO_3$ (420 mg, 2.47 mmol) were dissolved in ethylene glycol (50 mL) at room temperature. Concentrated HCl (1.43 mL, 17.3 mmol) was then added to this mixture and the reaction flask was moved to an oil bath with stirring and reflux for 20 min. The temperature of the oil bath was varied from 120 - 180 ºC to control the edge length of the AgCl nanocubes (see Figure 3.1). Prior to addition of the HCl, the solution was clear and nearly colorless. After

addition, the formation of a white precipitate gave a cloudy white mixture. The time for the appearance of precipitate varied from instantaneously at the highest reaction temperatures to about 8 min at the lowest.

Water (100 mL) was added to the mixtures obtained from the syntheses conducted at 180, 160 and 140 ºC and they were centrifuged (in 10-mL aliquots) for about 5, 20, or 30 min, respectively (at 1500 rpm). For the synthesis conducted at 120 ºC, a larger amount of H_2O (200 mL) was added to the mixture and it was centrifuged for about 40 min (at 1500 rpm). The white AgCl precipitates so obtained were washed with water, vacuum dried and weighed. The reaction yields were lowest (0.2001 g, 1.396 mmol, 57%) for the 120-ºC synthesis and higher (0.3150 – 0.3538 g, 2.198 – 2.470 mmol, 89-100%) for the syntheses conducted at higher temperatures.

3.2.3 Polyol Synthesis of Ag NWs

The Ag NW synthesis was scaled up tenfold from our previously published procedure.[2] PVP (3.34 g, 30.2 mmol) was dissolved in ethylene glycol (250 mL) and refluxed with stirring in an oil bath at 150 - 180 ˚C for 5 min. A previously prepared stock solution of AgCl nanocubes (0.23 mL, 0.24 mmol of AgCl) was injected into this hot reaction mixture and refluxed for 25 min. Then a $AgNO_3$ solution (10 mL, 0.12 M) was added dropwise at a rate of 25 mL/h while maintaining reflux and stirring. The work-up procedure employed was as previously described.[2]

3.2.4 Study of AgCl-nanocube Edge-length Effect on Ag-NW Diameter

AgCl nanocubes with various edge lengths were used for the Ag-NW synthesis previously reported that employs presynthesized AgCl nanocubes.[2] Stock solutions of AgCl nanocubes suspended in ethylene glycol (5 mL) were prepared at the concentrations listed in Table 1. The amount of stock solution added in each synthesis is also given in Table 1. The Ag-NW diameter

distributions produced by the syntheses were determined by SEM-image analysis, and are recorded in Figure 3.2.

Table 3.1 Concentrations of AgCl stock solutions prepared from syntheses described above and the μmol of AgCl nanocubes added to Ag NW polyol syntheses.

AgCl synthesis reaction temperature (ºC)	Mean edge length of AgCl nanocubes ± 1 st. dev.	Concentration of prepared AgCl stock solution (M)	μL of AgCl stock solution added to Ag-NW synthesis	μmol of AgCl added to Ag-NW synthesis
180	511 ± 64	0.476	50.7	24.1
160	291 ± 51	0.440	54.7	24.0
140	241 ± 74	0.494	47.9	23.6
120	83 ± 24	0.372	65.0	24.0

3.2.5 Determination of Ag^+ Reduction Kinetics[14]

The conversion of Ag^+ to Ag^0 as a function of time at various temperatures was determined gravimetrically by the following procedure. The growth of Ag NWs was initiated by the procedure given above for the polyol synthesis of Ag NWs. These studies were all conducted with AgCl nanocubes having a mean edge length of 100 ± 31 nm. Aliquots (5 mL) were removed by a volumetric pipet from the hot reaction mixture at regular intervals, beginning at the time the mixture became olive green in color. The Ag precipitate was extracted from each aliquot by adding water (5 mL) and centrifuging the mixture. The precipitate was then dried *in vacuo* and weighed. The mass obtained was multiplied by the inverse of the aliquot volume fraction and divided by the theoretical yield of Ag^0 to give the extent of conversion. The absolute errors expressed in Figures 3.3, 3.4 and 3.7 for the conversion of Ag^+ to Ag^0 was calculated by propagating the error in the measured Ag^0 mass. Scaling up the Ag NW synthesis reaction tenfold and using a volumetric pipet to collect aliquots minimized error in this gravimetric technique. This analysis assumes that the precipitate is pure Ag^0, which is

reasonable as the aqueous workup is known to remove PVP, and only small amounts of residual AgCl are present.[2] Each aliquot corresponded to 2% of the total volume. In total 10 – 12 aliquots were removed in each trial, corresponding to 20% of the total volume.

3.2.6 Determination of Ag-NW Growth Kinetics

The aliquots removed for the gravimetric determination of Ag^+ reduction kinetics (see above) were also used to obtain NW length and diameter distributions as functions of time and temperature. The Ag precipitates obtained from the aliquots were suspended in water and drop cast onto Si(111) wafers. The Ag-NW mean diameters and lengths in each aliquot were determined by SEM-image analysis, and are recorded in Table B3.1.

3.2.7 Reduction-Kinetics Trials Conducted with Other Additives

Reduction kinetics was determined in the presence of other additives to probe the nature of the induction period prior to Ag NW growth. The procedure described above was employed. Trials were conducted with the addition of glycolaldehyde dimer (3.14 g, 26.1 mmol) at 170 °C. Other trials were conducted with concentrated nitric acid (2.2 mL, 34.5 mmol) at 150 °C. In both sets of trials, the additive was injected all at once soon after the addition of AgCl nanocubes.

3.2.8 NMR monitoring of the Reaction of Ethylene Glycol and Nitric Acid

Ethylene glycol (2.6 mL, 46.5 mmol), concentrated nitric acid (22 μL, 0.345 μmol) and methylene chloride (22 μL, 0.345 μmol, as an internal standard) were combined at room temperature. An aliquot (20 μL) of this reaction mixture and d_6-DMSO (0.85 mL) were added to a 5-mm NMR tube. ^{1}H-NMR spectra were recorded to characterize the reaction products, as described in the Results (see also Figure B3.2).

3.3 Results

3.3.1 Polyol Syntheses Catalyzed by AgCl Nanocubes of Various Sizes

We adapted the method of Kim and coworkers[13] to the growth of AgCl nanocubes. The method employs the precipitation of AgCl upon combination of $AgNO_3$ and HCl in the presence of the polymeric stabilizer PVP. We found that the mean sizes of the AgCl nanocubes were readily controlled by the reaction temperature in the range of 120 – 180 °C (see Figure 3.1). The smallest nanocubes having a mean edge length ± one standard deviation of 83 ± 24 nm were obtained at the lowest temperature (120 °C), whereas the largest (511 ± 64 nm) were obtained at the highest temperature (180 °C). A plot of mean edge length vs. synthesis temperature (Figure 3.1e) showed that the size range was sufficiently large, and the size distributions sufficiently narrow, to provide distinct AgCl-nanocube populations for use in probing for a heterogeneous-catalyst size effect.

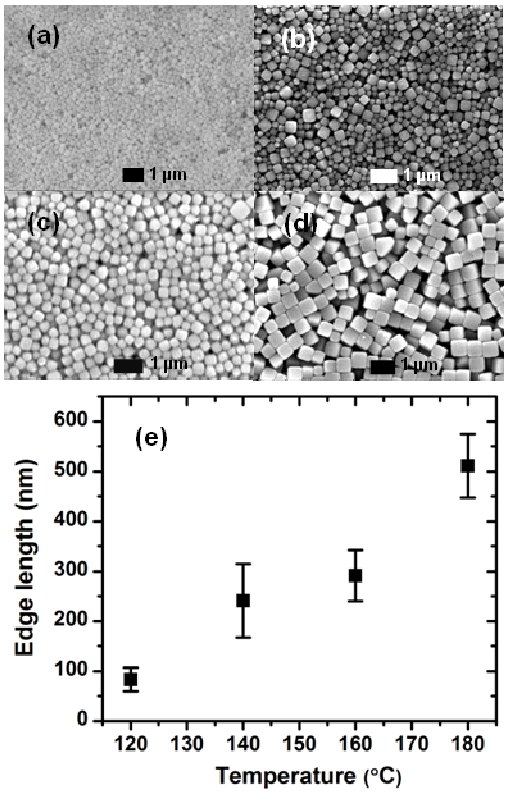

Figure 3.1 SEM images of AgCl nanocubes synthesized at different reaction temperatures, and their mean edge lengths ± one standard deviation; (a) 120 °C, 83 ± 24; (b) 140 °C, 241 ± 74; (c) 160 °C, 291 ± 51; (d) 180 °C, 511 ± 64. (e) Plot of nanocube mean edge length vs. synthesis temperature. The error bars are ± one standard deviation in the size distribution.

The four AgCl-nanocube size populations obtained as described above were separately used to catalyze Ag-NW growth, by the method we reported previously employing pre-synthesized AgCl nanocubes.[2] These reactions were conducted at 180 °C, and at a smaller scale than reported here for the reduction-kinetics trials. The amount (moles) of added AgCl was held constant in each trial, such that the number of AgCl nanocubes in reactions employing smaller nanocubes was larger than the number of AgCl nanocubes in reactions employing larger nanocubes. After a total reaction time of 70 min, the NWs were collected and their diameter distributions determined.

The diameter data are plotted as Ag-NW mean diameter vs. the AgCl-nanocube size in Figure 3.2. By analogy to the other catalyzed nanowire growth methods, VLS and SLS growth,[5-8] if the Ag-NW diameters scaled with the size of the catalyst particle, the diameters would be expected to increase with the increasing size of the catalyst. However, the scatter in the diameter data (Figure 3.2) revealed no strong correlation between Ag-NW diameter and AgCl-nanocube size. The results established that the NW diameters do not depend on the size of the heterogeneous nucleant from which they grow, and that another effect or effects determine the Ag-NW diameters.

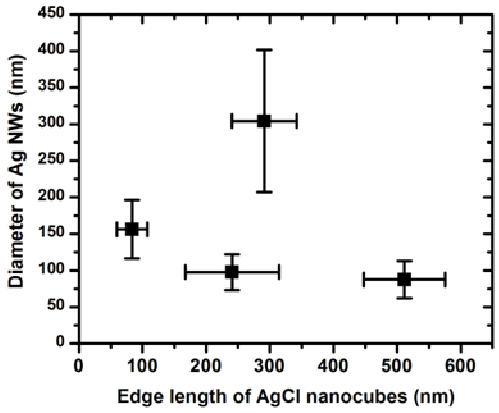

Figure 3.2 Plot of Ag-NW mean diameter vs. AgCl nanocube mean edge length. The error bars are ± one standard deviation in each size distribution. The Ag-NW mean diameters, from the shortest AgCl-nanocube edge length to the longest, are 156 ± 40, 98 ± 24, 304 ± 97 and 87 ± 26 nm.

3.3.2 Kinetic Profiles of the Ag^+ Reduction Process

The growth of Ag NWs was conducted as described above using AgCl-nanocube heterogeneous nucleants having a mean edge length of 100 ± 31 nm. The gravimetric method of Wiley and coworkers[14] was adapted to determine the extent of the conversion of Ag^+ to Ag^0 as a function of time and temperature. The conversion kinetics, plotted in Figure 3.3, exhibit sigmoidal profiles with temperature-dependent induction periods. The fits to the kinetic data by the Avrami equation (eq 1) are to guide the eye, and are not physically meaningful.

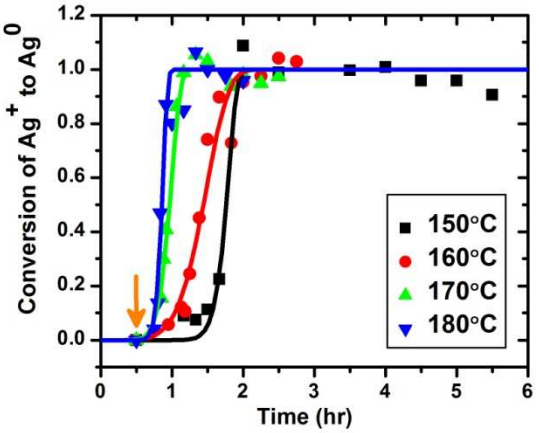

Figure 3.3 Plots of the conversion of Ag^+ to Ag^0 vs. reaction time at various temperatures, with eq-1 fits to guide the eye. These fits are not physically meaningful, as the fit function was not derived for the reduction kinetics. The inset legend identifies the data at each reaction temperature. The orange arrow identifies the time at which the dropwise addition of $AgNO_3$ commenced in each trial. The error in each data point is smaller than the symbol size.

We note that $AgNO_3$ addition was begun at 30 minutes. In the initial 30-minute period prior to $AgNO_3$ addition, the AgCl nanocubes were heated at the reaction temperature in the ethylene glycol/PVP solution, resulting in the reduction of small amounts of Ag^+ from the AgCl nanocubes to form Ag clusters or small nanoparticles on the nanocube surfaces. This step primed the AgCl nanocubes for the growth of Ag NWs.[2] The induction period was defined as the time between the start of $AgNO_3$ addition and the visual observation of Ag-NW formation, indicated by the appearance of grey, opalescent swirls in the reaction mixture.[2] The induction periods defined in this way ranged from 17 ± 5 min at 180 °C to 60 ± 2 min at 150 °C (Figure 3.4b), and corresponded closely to the upturns in the reduction kinetics evident in Figure 3.3.

We surmised that these induction periods were associated with the formation of the active reducing agent. A previous study identified glycolaldehyde, an oxidation product of ethylene glycol, as the Ag^+ reductant.[15] The polyol synthesis is conducted under an ambient (O_2-containing) atmosphere, and the rate of glycolaldehyde formation was shown to increase with

increasing temperature.[15] The decrease in the induction period with increasing temperature (Figure 3.4b) was consistent with glycolaldehyde serving as the reducing agent.

To further establish the correlation of the induction period with the formation of glycolaldehyde, experiments were conducted with the initial addition of glycolaldehyde dimer (the commercially available form of glycolaldehyde). We reasoned that addition of glycolaldehyde from the outset should significantly shorten the induction period. However, we observed that addition of glycolaldehyde dimer shortened the induction period only slightly at 170 °C (reducing it from 22 to 20 min). Additionally, the selectivity for NW formation was lost (Figure B3.3). We concluded that the dimer was less potent as a Ag^+ reductant than monomeric glycolaldehyde, and that the dimer did not readily dissociate to monomer under the conditions employed.

In a second set of experiments to probe the origin of the induction period, HNO_3 was added to the polyol synthesis at the outset. Figure 3.4a plots the reduction kinetics at 150 °C with added HNO_3, at 150 °C without added HNO_3, and at 180 °C without added HNO_3, for comparison. The induction period at 150 °C with added HNO_3 determined visually (see above) was 10 min, shorter than that at 180 °C without added HNO_3 (17 min), and much shorter than that at 150 °C without added HNO_3 (60 min, Figure 3.4b). Additionally, the upturn (Fig. 3.4a) in the reduction kinetics (associated with the induction period) in the presence of HNO_3 was extremely rapid after the initial 30-min stirring period prior to the dropwise addition of $AgNO_3$. Thus, the added HNO_3 significantly shortened the induction period.

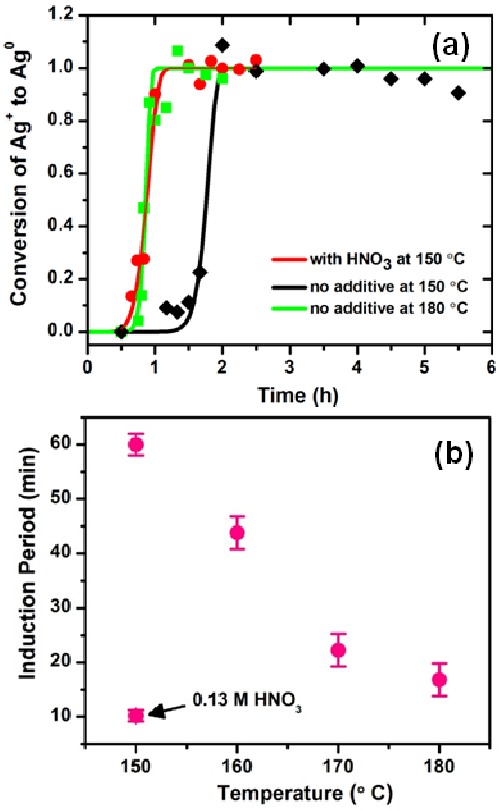

Figure 3.4 (a) Plots of the conversion of Ag^+ to Ag^0 vs. reaction time with HNO_3 at 150 °C, without added HNO_3 at 150 °C and without added HNO_3 at 180 °C, with eq-1 fits. The error in each data point is smaller than the symbol size. (b) Plot of induction period vs. temperature with no additives and with HNO_3 added (indicated by arrow) at 150 °C. The error bars are ± one standard deviation in induction time as observed from multiple trials at each temperature.

To understand the role of the added HNO_3, an ethylene glycol solution of HNO_3 at the concentration employed above was heated at 150 °C for a few minutes, and then cooled. After addition of an internal standard, ^1H NMR spectra (Figure B3.2) were obtained that provided clear evidence for the formation of monomeric glycolaldehyde in amounts larger than stoichiometrically required for the complete reduction of Ag^+ under the conditions of the polyol synthesis. Thus, HNO_3 is sufficiently oxidizing to convert ethylene glycol to glycolaldehyde. A proposed pathway for the oxidation is given in Scheme B3.1. We concluded that the added HNO_3 rapidly generated monomeric glycolaldehyde, the reducing agent for the polyol process, thus dramatically shortening the induction period (to 10 min from 60 min).

The generation of glycolaldehyde within a few minutes after HNO_3 addition may suggest that the induction period should have been eliminated entirely, and thus have been less than the observed 10 min. SEM images obtained near the end of this the induction period (at 9 min) showed shorter Ag nanorods rather than NWs (Figure B3.4), indicating that NW growth was just commencing. The result suggested that most of the residual 10-min induction period was a nucleation-like period, the time required for nucleation of the Ag NWs. In the Discussion, we will argue that this induction period was the time required for the initially formed Ag nanoparticles (on the AgCl nanocubes) to grow beyond the critical size[16] for pentagonal twinning. Thus, the experiments with added HNO_3 described here associate the longer induction periods under normal polyol-synthesis conditions (without the HNO_3 additive) with the generation of glycolaldehyde.

After the induction period, the reduction process occurred rapidly at all temperatures (see Figure 3.3). This reduction reaction has been previously described as autocatalytic,[15] which is consistent with our results in Figure 3.3. In the polyol synthesis under standard conditions, no glycolaldehyde-generating nitric acid is initially present, and glycolaldehyde forms only by a slow, adventitious air oxidation. However, Wiley and coworkers have proposed that the reduction process itself produces protons according to eq 2,[14] and we note that nitrate ions are also present from the $AgNO_3$ precursor, providing the equivalent of nitric acid. Consequently the nitric acid generated by the reduction reaction in eq 2 rapidly produces glycolaldehyde reductant in progressively increasing amounts as the reduction process proceeds, explaining its autocatalytic character. Thus, the sigmoidal kinetics result from an initial induction period associated with the formation of initial quantities of glycolaldehyde by adventitious oxidation,

followed autocatalytic generation of glycolaldehyde as the Ag^+ reduction continues to completion.

$$HOCH_2CHO + 2Ag^+ + H_2O \longrightarrow HOCH_2COOH + 2Ag^0 + 2H^+ \qquad (2)$$

3.3.3 Ag NW Diameter and Length Growth Kinetics

Having established the time scales for the reduction process (see the text above and Figure 3.3), we next sought to compare the reduction kinetics to the Ag-NW growth kinetics in mean diameter and length. SEM images were obtained from the same aliquots removed in the reduction-kinetics trials, and were analyzed to determine the length and diameter distributions as functions of time and temperature. Representative images are shown in Figure 3.5, using data collected from a 180-°C trial.

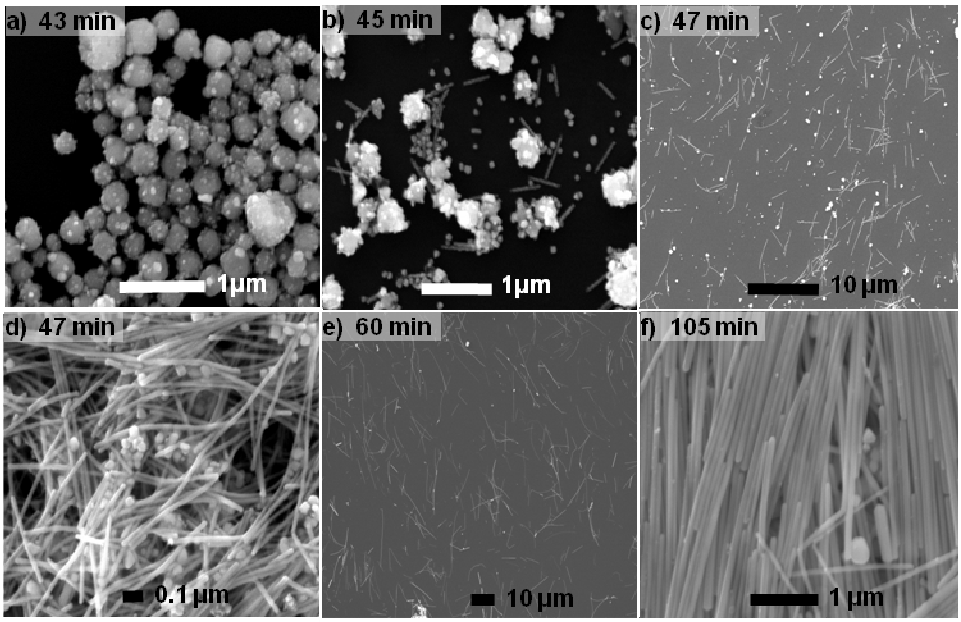

Figure 3.5 SEM images of aliquots taken at a) 43 min, b) 45 min, c) and d) 47 min, e) 60 min and f) 105 min from Ag NW synthesis reaction at 180 ºC.

Early time images (Figure 3.5a, b) collected during the induction period showed the initiation of NW growth at around 45 min. The Figure 3.5b NWs were not affixed to AgCl nanocubes, because they were nucleated by the smallest nanocubes, which were consumed by the initial growth process. (However, see Figure B3.1 for images of Ag NWs growing from a batch of larger AgCl nanocubes.) Only the larger AgCl nanocubes from the size distribution (mean edge length 100 ± 31 nm), which are poorer heterogeneous nucleants of Ag NWs,[2] are evident in Figure 3.5b.

Representative images from the rapid growth period are included in Figure 3.5c – f. Images were collected at both low and high NW densities for determinations of mean lengths and diameters, respectively. During this period the larger AgCl nanocubes were also consumed, undergoing reduction to metallic Ag.

The data plotted in Figure 3.6 were scaled by the final (limiting) mean diameter and length for each trial ($\bar{d}(t)/\bar{d}_{\mathrm{lim}}$ and $\bar{l}(t)/\bar{l}_{\mathrm{lim}}$), such that the *y* axes scale from 0 to 1. This normalization was to facilitate comparison of the kinetics at the various temperatures. The final mean diameters and length were determined by averaging several of the late-time points at the conclusion of growth, and are recorded in Table B3.1. The data were fit by eqs 3 and 4, and the resulting curves are to guide the eye.

$$\frac{\bar{l}(t)}{\bar{l}_{\mathrm{lim}}} = \left[1 - \exp\left\{-\left(k_{\mathrm{g}}t\right)^{n}\right\}\right] \qquad (3)$$

$$\frac{\bar{d}(t)}{\bar{d}_{\mathrm{lim}}} = \left[1 - \exp\left\{-\left(k_{\mathrm{g}}t\right)^{n}\right\}\right] \qquad (4)$$

Figure 3.6a reveals considerable scatter in the later-time mean-length data. Moreover, a steady decrease in mean length was evident in the later-time data obtained at 180 °C. We note that the reaction mixtures were stirred during Ag-NW growth, and that the SEM specimens were

dispersed by sonication. We suspect that mechanical contact between NWs during stirring and sonication may have caused some breakage, reducing the apparent mean lengths. Breakage during sonication would occur in a stochastic manner, producing the later-time scatter. Stirring-induced contact would have been most extreme at the highest reaction temperature, explaining the apparent shrinkage of the mean lengths after completion of growth at 180 °C.

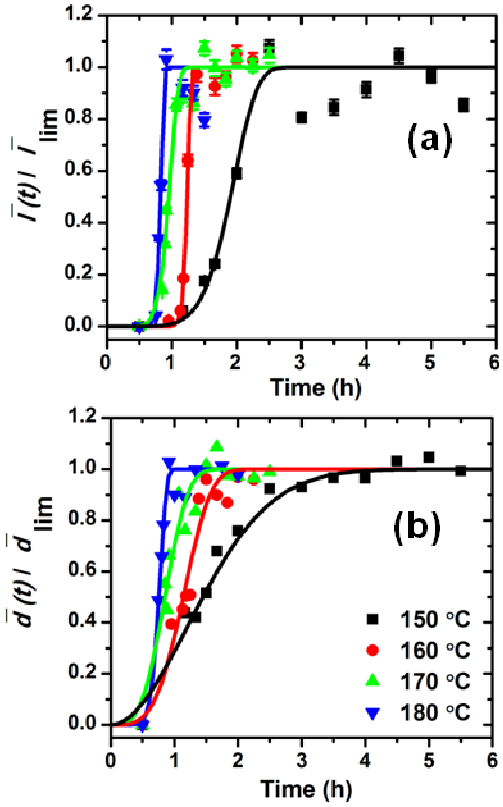

Figure 3.6 Plots of growth kinetics in normalized mean (a) length ± one st. error of mean with eq-3 fits and (b) diameter ± one st. error of mean with eq-4 fits as function of reaction time. Error bars are shown, but the error in most of the data points is smaller than the symbol size.

The Figure 3.6 data show that the rates of growth in both length and diameter increase with increasing temperature, as expected. The delays in the upturn in the mean length data (Figure 3.6a) at the lower temperatures of 150 and 160 °C are associated with the induction periods observed visually, and are consistent with the delayed upturns evident in Figures 3.3 and 3.4.

Interestingly, if there were initial kinetic delays in the diameter data (Figure 3.6b) associated with the induction periods, they were not captured in our data. At all temperatures, the first data point collected after the initiation of dropwise $AgNO_3$ addition showed that the mean diameter had rapidly grown to about 40% of its final value within this brief early period. At the same early times, the growth in mean lengths was 10% or less of their final values. The possible mechanistic significance of the rapid early growth in diameter is explored in the Discussion.

Figure 3.7 directly compares the growth kinetics in NW diameter and length at a representative temperature (170 °C; similar plots at the other growth temperatures are Figures B3.5-B3.7). In Figure 3.7a, the two *y* axes (left and right) are adjusted to overlay the final mean diameter and length points, thus scaling the growth curves together. The two curves are very similar, showing that, apart from the early rapid diameter increase, the growth in diameter and length occurred over the same time scale. That is, the growth in diameter and length were approximately proportional. Figure 3.7b plots the growth kinetics in diameter and length on the same scale (single *y* axis), emphasizing that the absolute growth in length was greater than that in diameter by two orders of magnitude.

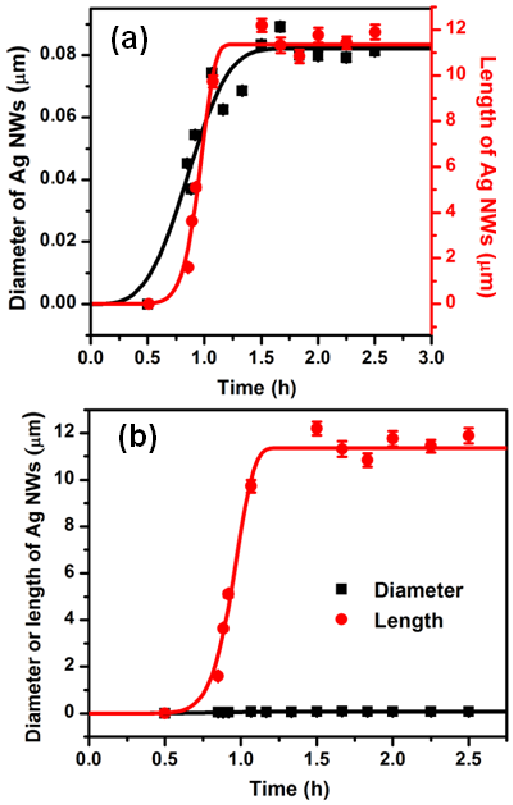

Figure 3.7 Plots of time-dependent growth in length and diameter of Ag NWs at 170 ºC on (a) relative y-axis scales and (b) an absolute (single) y-axis scale. The error bars are ± one st. error of mean in each data point. Error bars are not visible where the error is smaller than the symbol size.

Figure 3.8 compares the growth in NW length, diameter, aspect ratio, and volume to the kinetics of the Ag^{+}-reduction process (at 170 °C; similar plots at the other growth temperatures are Figures B3.8-B3.10). On each plot, the *y*-axis scaling is adjusted to overlay the final values on two curves. In each of the four comparisons (Fig. 3.8a-d), the two relatively scaled curves parallel one another fairly closely, showing that the growth in NW length, diameter, aspect ratio, and volume followed the extent of the reduction reaction. The time scales for the reduction process and NW growth in the four parameters presented here were essentially the same.

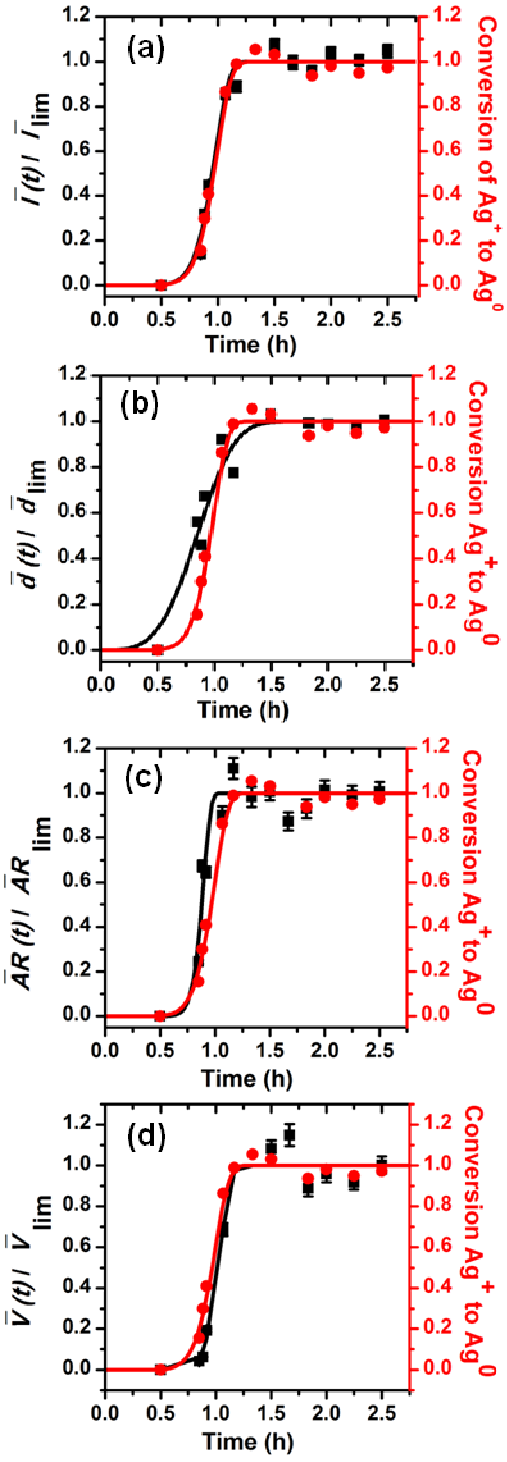

Figure 3.8 Plots of conversion of Ag^{+} to Ag^{0} with growth kinetics. Normalized mean (a) length with eq-3 fit, (b) diameter with eq-4 fit, (c) aspect ratio (AR) with the corresponding fit and (d) volume with the corresponding fit. Each of a-d includes the eq-1 fit and is plotted as a function of reaction time at 170 °C. The error bars are ± one st. error of mean in each data point. Error bars are not visible where the error is smaller than the symbol size.

3.4 Discussion

We considered two limiting possibilities in discerning the growth mechanism for the polyol synthesis of Ag NWs. In one limiting possibility, the reduction kinetics would be significantly faster than the growth kinetics in Ag-NW diameter and length. In that event, the reduction process would presumably generate populations of small Ag^0 clusters or nanoparticles, which would subsequently produce NWs by aggregation and/or Ostwald ripening. In the second limiting possibility, the growth kinetics would closely parallel the reductions kinetics, indicating that NW growth was controlled or limited by the reduction process, excluding significant contributions by aggregation or Ostwald ripening. That is, if the growth in either NW length or diameter lagged significantly behind the Ag^+ reduction rate, that would constitute evidence for the participation of either aggregation or ripening in the growth process.

We consider the close parallels between the reduction and growth kinetics evident in Figure 3.8 to rule out significant contributions of nanoparticle/nanocluster aggregation or Ostwald ripening to the growth mechanism. If either of the latter processes were responsible for NW growth, then the reduction kinetics should occur over a detectably shorter time scale than growth, as both require the initial formation of nanoclusters and/or nanoparticles.

The data (Figure 3.7) also reveal the steady, uniform growth in *both* length and diameter over the course of the reduction process. That is, deposition of Ag on the growing NWs does not occur exclusively at the tip, lengthening the NWs, but also on the sidewalls, steadily increasing their diameters as well. Figure 3.7b shows that the deposition kinetics on the tips are much more rapid than on the sidewalls in an absolute sense, which has been attributed to the higher surface energies of the pentagonally twinned tip facets.[17] However, in a relative sense (Figure 3.7a), the

time scales for the growth in length and diameter are nearly (but not exactly) the same. The results suggest that growth occurs by Ag-NW surface-catalyzed reduction on *all* surfaces concurrently, on the tip facets *and* the sidewall facets.

The results discussed here suggest that the surface-catalyzed reduction is the rate-limiting step in the NW-growth process. To verify that conclusion, we compare the experimental reduction rates and an experimental activation energy to those expected for a diffusion-controlled process. To be rate limiting, the reduction rates and activation energy must be smaller and larger, respectively, than those associated with Ag^+ diffusion to the growing NWs. As detailed in the Appendix B, the experimentally observed reduction rates are 13 orders of magnitude smaller than the predicted diffusion-controlled rates. Moreover, the experimentally determined activation energy of 138.5 kJ/mol at 150 °C is much larger than a predicted value of 23.7 kJ/mol at 150 °C for a diffusion-controlled reaction (Appendix B). Additionally, our experimental activation energy is much higher than the experimental activation energy for the diffusion-controlled growth of Cu NWs of 11.5 kJ/mol at 70 °C determined by Wiley and coworkers.[18] These comparisons strongly support the conclusion that the surface-catalyzed reduction is rate limiting.

Figures 3.6 and 3.7a also indicate that the initial growth in diameter *precedes* growth in length, such that the Ag NWs have achieved about 40% of their final diameters at the time that NW lengthening commences. Given the final NW diameters measured (Table B3.1), the kinetic results suggest that initially formed Ag nanoparticles must reach a critical size in the range of 20-30 nm prior to the onset of growth in the length dimension. Moreover, the smallest NW mean diameter we measured at the earliest stages near the onset of growth was 23 nm (Figure B3.4). Prior work by Gai,[17] Xia,[11] and others has established that the NWs grow from pentagonally

twinned nanoparticles. Marks has determined that single-crystal Ag nanoparticles transition to pentagonally twinned structures only after they grow beyond a critical size of 10 nm (*in vacuo*).[16] Under our reaction conditions, we surmise this critical size to be in the range of 10-30 nm.

Thus the initial growth in diameter proceeds until the initially generated nanoparticles become large enough to form pentagonal twins, at which point lengthening commences by deposition on the twinned tip facets. We attribute the residual 10-min induction period observed even in the presence of added HNO_3 to the time necessary for the initially formed Ag nanoparticles, which are heterogeneously nucleated on the AgCl nanocubes, to grow beyond the critical size for pentagonal twinning. The longer induction periods (at the lower temperatures) in the absence of added HNO_3 are due to the longer time needed to generate the glycolaldehyde reducing agent by adventitious oxidation.

Because the NW diameter grows continuously throughout the Ag^+ reduction reaction, the diameter is not fixed at the time of NW nucleation, as it is, for example, in the heterogeneously catalyzed SLS[8] and VLS[5-7] NW growth mechanisms. Consequently, the final mean Ag NW diameter in this polyol synthesis bears no relation to the size of the AgCl-nanocube heterogeneous nucleant employed, and cannot be controlled by nucleant size. Rather, the final mean diameter is determined by nucleation density, amount of Ag^+ precursor, and reaction time. Wiley and coworkers[15] have controlled nucleation density with reaction temperature, and have so asserted some control over mean Ag-NW diameter and length, which together scale proportionally with nucleation density. Alternatively, Chou and coworkers[19] have systematically varied Ag-NW mean diameters with added chloride ion, which preferentially binds the side-wall facets, inhibiting growth in diameter. This latter surface-poisoning strategy seems most

promising for independently controlling Ag-NW mean diameter and length in the polyol synthesis.

3.5 Conclusions

A previous study established that the growth of Ag NWs by the polyol process is heterogeneously catalyzed by Ag halide nanocubes.[2] The present work demonstrates that the diameters of the Ag NWs are not fixed by this heterogeneous nucleation process, but rather growth continuously over the time scale of the reaction. Kinetics studies show that NW diameters and lengths grow concurrently, and that both are limited by the extent of the Ag^{+}-reduction process. The results are consistent with a rate-limiting surface-catalyzed reduction reaction occurring on all side-wall and tip facets of the growing Ag NWs, and rule out significant contributions by nanoparticle aggregation or Ostwald ripening.

3.6 References

35. Ducamp-Sanguesa, C.; Herrera-Urbina, R.; Figlarz, M. *J. of Solid State Chem.* **1992**, *100*, 272-280.

36. Schuette, W. M; Buhro, W. E. *ACS Nano* **2013**, *7*, 3844-3853.

37. Li, Z. C.; Shang, T. M.; Zhou, Q. F.; Feng, K. *Micro & Nano Letters* **2011**, *6*, 90-93.

38. Coskun, S.; Aksoy, B.; Unalan, H. E. *Cryst. Growth Des.* **2011**, *11*, 4963-4969.

39. Cui, Y.; Lauhon, L. J.; Gudiken, M. S.; Wang, J.; Lieber, C. M. *Appl. Phys. Lett.* **2001**, *78*, 2214-2216.

40. Gudiken, M. S.; Wang, J.; Leiber, C. M. *J. Phys. Chem. B* **2001**, *105*, 4062-4064.

41. Wu, Y.; Yang, P. *J. Am. Chem. Soc.* **2001**, *123*, 3165-3166.

42. Wang, F.; Dong, A.; Sun, J.; Tang, R.; Yu, H.; Buhro, W.E. *Inorg. Chem.* **2006**, *45*, 7511-7521.

43. Viau, G.; Piquemal, J. Y.; Esparrica, M.; Ung, D.; Chakroune, N.; Warmont, F.; Fiévet, F. *Chem. Commun.* **2003**, *17*, 2216-2217.

44. Giersig, M.; Pastoriza-Santos, I.; Liz-Marzán, L. M. *J. of Mater. Chem.* **2004**, *14*, 607-610.

45. Sun, Y.; Mayers, B.; Herricks, T.; Xia, Y. *Nano Lett.* **2003**, *3*, 955-960.

46. Abramoff, M.D.; Magalhaes, P.J.; Ram, S.J. *Biophotonics International* **2004**, *11*, 36-42.

47. Kim, S.; Chung, H.; Kwon, J. H.; Yoon, H. G.; Kim, W. *Bull. Korean Chem. Soc.* **2010**, *31*, 2918-2922.

48. Bergin, S. M.; Chen, Y.; Rathmell, A. R.; Charbonneau, P.; Li, Z.; Wiley, B. J. *Nanoscale* **2012**, *4* , 1996-2004.

49. Skrabalak, S. E.; Wiley, B. J.; Kim, M.; Formo, E. V.; Xia, Y. *Nano Lett.* **2008**, *8*, 2077-2081.

50. Marks, L. D. *Ultramicroscopy* **1985**, *18*, 445-452.

51. Gai, P. L.; Harmer, M. A. *Nano Letters.* **2002**, *2*, 771-774.

52. Ye, S.; Chen, Z.; Ha, Y. C.; Wiley, B. J. *Nano letters*, **2014**, *14*, 4671-4676.

53. Chang, Y. - H.; Lu, Y. - C.; Chou, K. - S. *Chemistry Letters* **2011**, *40*, 1352-1353.

Chapter 4

4.1 Conclusion

The roles of the halide additive in the polyol synthesis is poorly understood, yet its addition was shown to be crucial to Ag NW growth.[1] In this study, we show that the halide additive in the polyol synthesis of Ag NWs forms silver halide nanocubes in solution which then heterogeneously nucleate Ag NWs from its surfaces. The smaller sized nanocubes (edge lengths smaller than about 150 nm) are more potent nucleating agents than the larger sized (edge length of 200-600 nm) nanocubes. The AgCl nanocube is used up early on in the synthesis reaction and contributes to the growth the Ag NWs. The concentration of the AgCl nanocubes affects the final lengths of the Ag NWs while the edge length of the AgCl nanocubes has no effect on the final diameters of the Ag NWs. At smaller AgCl nanocube concentrations the Ag NWs are longer as compared to reactions with larger AgCl nanocube concentrations where the Ag NWs are shorter.

Another aspect of the polyol synthesis of Ag NWs that is poorly understood is the mechanistic features controlling length and diameter. There is disagreement in the literature about the fundamental aspects of growth of Ag NWs. Ostwald ripening[2] or alternatively, aggregative growth[3] was proposed to be proposed growth mechanism. In this study, we show that in the polyol synthesis, Ag NWs grow by a surface-reduction rate –limited growth.

The diameters and lengths of the Ag NWs are shown to increase until the reduction reaction was complete. The S-shaped reduction kinetics curves are characterized by a temperature-dependant induction period followed by a rapid autocatalytic reduction period and finally the completion of the reduction reaction when the precursor is completely used up. The diameter and length growth kinetics also exhibit similar S-shaped curves.

The reduction reaction is rate limited by the temperature -dependent adventitious generation of the reductant glycolaldehyde. This time period required to generate glycolaldehyde in solution contributes to the induction period prior to the onset of wire growth. In the presence of excess glycolaldehyde, a 10-minute induction still exists which is attributed to the time needed for the silver clusters (on the surface of the AgCl nanocube) to grow beyond a critical size of 10-30 nm and transition into a multiply twinned particle, active for nanowire growth.

The large activation energy barrier of 138.5 kJ/mol and the small reaction rate constant of 2.11×10^{-4} s^{-1} are calculated at 150 ºC for the reduction reaction. This supports the conclusion that the reduction reaction is not diffusion controlled but is instead limited by the reduction reaction on the surface of the growing Ag NW. In case of diffusion-controlled growth, limited by the diffusion of Ag^{+} ions towards the surface of the Ag NW the reaction would be characterized by lower activation energies, lower diffusional rate constants and larger reduction rate constants. The growth kinetics of length and diameter closely parallel the reduction kinetics, providing additional evidence for the surface-reduction rate-limited growth. The diameter of the Ag NW is shown to increase throughout the reduction process and therefore cannot be controlled by the size of the heterogeneous AgCl nucleant. Building upon strategies listed in this thesis additional studies need to be done to grow Ag NW with controllable aspect ratios.

4.2 Future Work

The need for electrically conductive and optically transparent materials is expanding due to the increased use of optoelectronic devices, solar cells, and liquid crystal displays. Indium-tin-oxide (ITO) is the most widely used material due to its low sheet resistance (<100 Ω /sq) and high transmittance (~90%).[4] Some alternatives to ITO are single-walled carbon nanotubes,[5] graphenes[6], and Ag NW films.[4] CNT networks have a higher sheet resistance 200-1000 Ω /sq with optical transmittance of 80-90%, while graphene electrodes have ~300 Ω /sq resistance and 80% transmittance.[4] Ag NW films were shown be better than the best ITO samples with 20 Ω /sq resistance and 80% transmittance.[4] Ag NW films were superior also due to their good robustness to repeated bending which is a problem in for the brittle ITO films.[4] Ag NW films are thus a good alternative to ITO films for replacement in electronics and solar cells. However, these attractive features of the Ag NW films are strongly dependent on the nanowire dimensions.

We showed how the length of Ag NWs can be controlled by varying the concentration of the AgCl nanocubes in Chapter 2. In this study, the size ranges for the shorter Ag NWs were 1-6 μm and the size range for the longer Ag NWs were 3-19 μm. A systematic study should be performed varying $AgNO_3$ and AgCl nanocube concentrations to try to achieve a narrower size range of final Ag NW lengths.

The average final diameters of the Ag NWs synthesized in this study were 70 nm, independent of reaction temperature. The surface poisoning strategy with the addition of excess halide ions seems to be a promising route to control the diameter of the Ag NWs.[7] Further investigation needs to be done to determine effects of the different halide ions at varying concentrations and temperatures on the final diameters of the Ag NWs. The mechanism as to

why the addition of a Cl^- ion, only yields wires as thin as 55 nm is also unclear.[7] The correct timing of addition of the halide ion into the reaction mixture to minimize formation of junk nanoparticles that are poor nucleants also needs to be investigated. Subsequently, the adsorption mechanism of the halide ion to the Ag NW surface needs to be studied using surface adsorption models. Some other methods of synthesizing Ag NWs as thin an 40 nm have been reported by using PVP of various lengths simultaneously in solution.[8] This method needs can also be adapted to study ways of growing Ag NWs with diameters less than 40 nm.

4.3 References

54. Coskun, S.; Aksoy, B.; Unalan, H. E. *Cryst. Growth Des.* **2011**, *11*, 4963-4969.

55. Sun, Y.; Mayers, B.; Herricks, T.; Xia, Y. *Nano Lett.* **2003**, *3*, 955-960.

56. Viau, G.; Piquemal, J. Y.; Esparrica, M.; Ung, D.; Chakroune, N.; Warmont, F.; Fiévet, F. *Chem. Commun.* **2003**, *17*, 2216-2217.

57. Hu, L.; Kim, H. S.; Lee, J. Y.; Peumans, P.; Cui, Y. *ACS Nano* **2010**, *4*, 2955-2963.

5. Wu, Z.; Chen, Z.; Du, X.; Logan, J. M.; Sippel, J.; Nikolou, M.; Kamaras, K.; Reynolds, J. R.; Tanner, D. B.; Hebard, A. F.; Rinzler, A. G. *Science* **2004**, *305*, 1273-1276.

6. Kang, J.; Kim, H.; Kim, K. S.; Lee, S. K.; Bae, S.; Ahn, J. H.; Kim, Y.-J.; Choi, J.-B.; Hong, B. H. *Nano Lett.* **2011**, *11*, 5154-5158.

7. Chang, Y. - H.; Lu, Y. - C.; Chou, K. - S. *Chem. Lett.* **2011**, *40*, 1352-13532.

8. Ran, Y.; He, W.; Wang, K.; Ji, S.; Ye, C. *Chem.Comm.***2014,** *50*, 14877-14880.

Appendix A

Additional Figures for Chapter 2

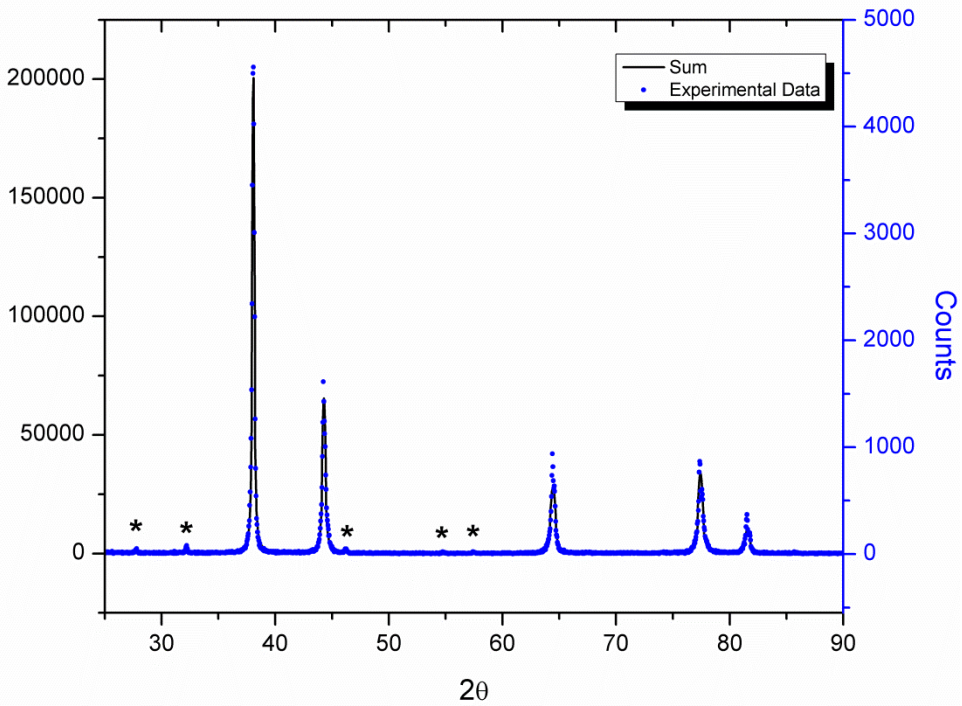

Figure A2.1 The blue points are XRD data collected from synthesized Ag NWs from a reaction with low NaCl concentration and using ethylene glycol from Aldrich. Refinement of this pattern performed using Powdercell 2.4[32] yielded the calculated pattern represented by the underlying black curve and the volume percent of Ag (97.4%) and AgCl (2.6%). Asterisks identify reflections from AgCl.

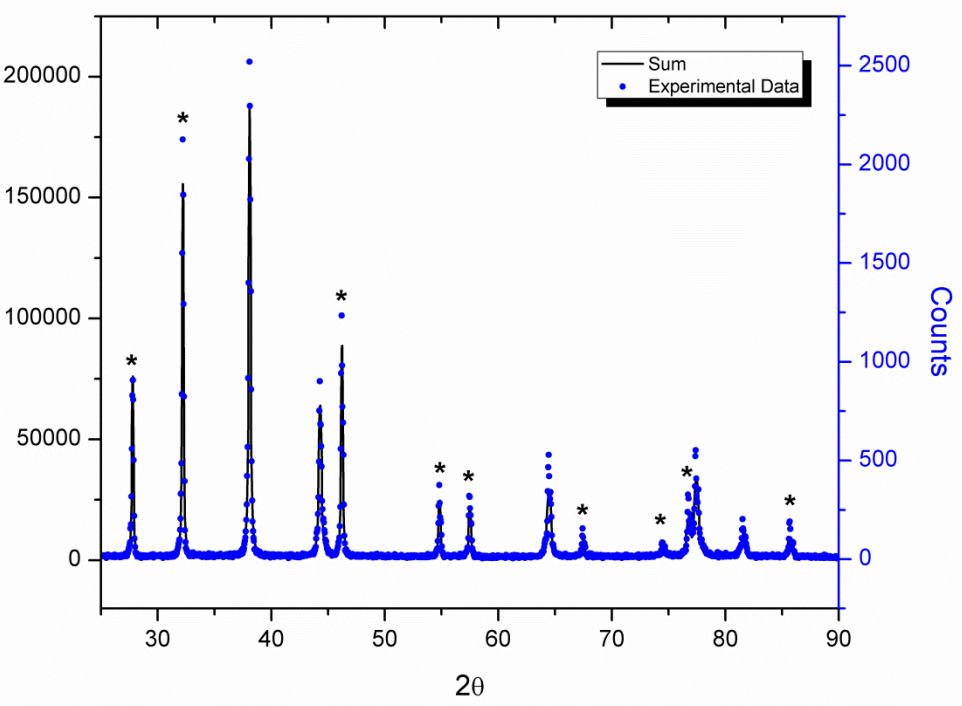

Figure A2.2 The blue points are XRD data collected from Ag NWs synthesized from a reaction with high NaCl concentration and using ethylene glycol from Aldrich. Refinement of this pattern performed using Powdercell 2.4[32] yielded the calculated pattern represented by the underlying black curve and the volume percent of Ag (34.8%) and AgCl (64.2%). Asterisks identify reflections from AgCl.

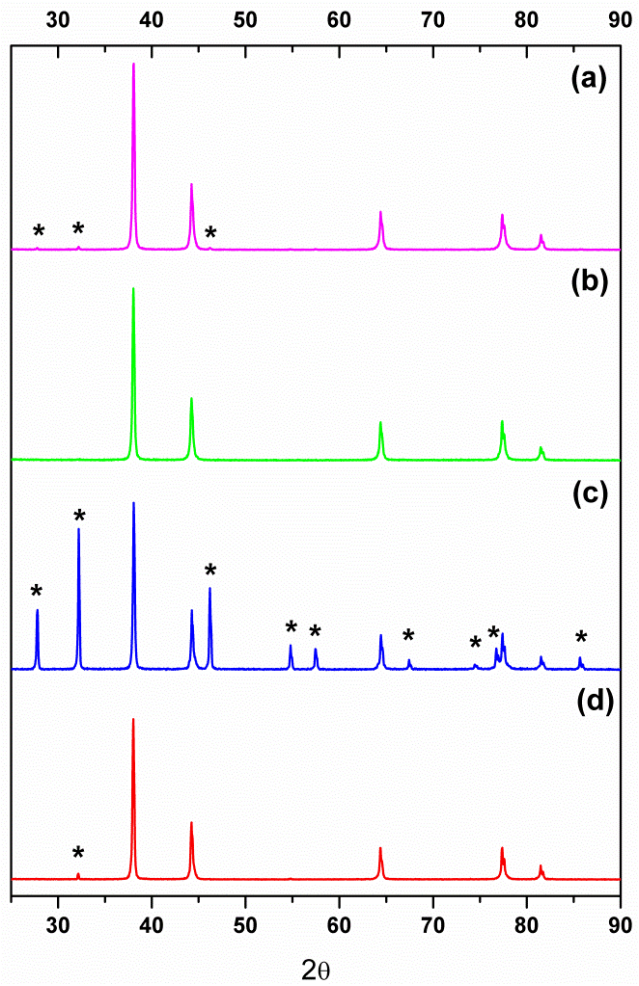

Figure A2.3 XRD patterns of Ag NWs from a reaction using low NaCl concentration before (a) and after (b) washing the Ag NWs with NH_4OH. XRD patterns of AgNWs from a reaction using high NaCl concentration before (c) and after (d) washing the Ag NWs with NH_4OH. Asterisks identify reflections from AgCl.

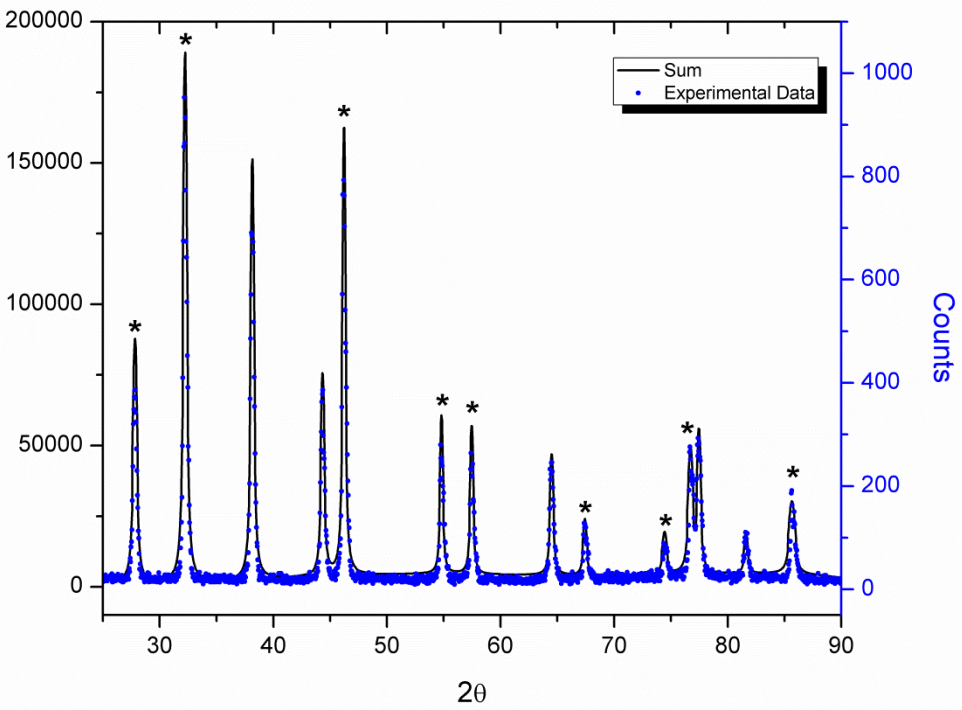

Figure A2.4 The blue points are XRD data collected from the byproduct lump obtained from a reaction with low NaCl concentration and using ethylene glycol from J. T. Baker. Refinement of this pattern performed using Powdercell 2.4[32] yielded the calculated pattern represented by the underlying black curve and the volume percent of Ag (19.6%) and AgCl (80.4%). Asterisks identify reflections from AgCl.

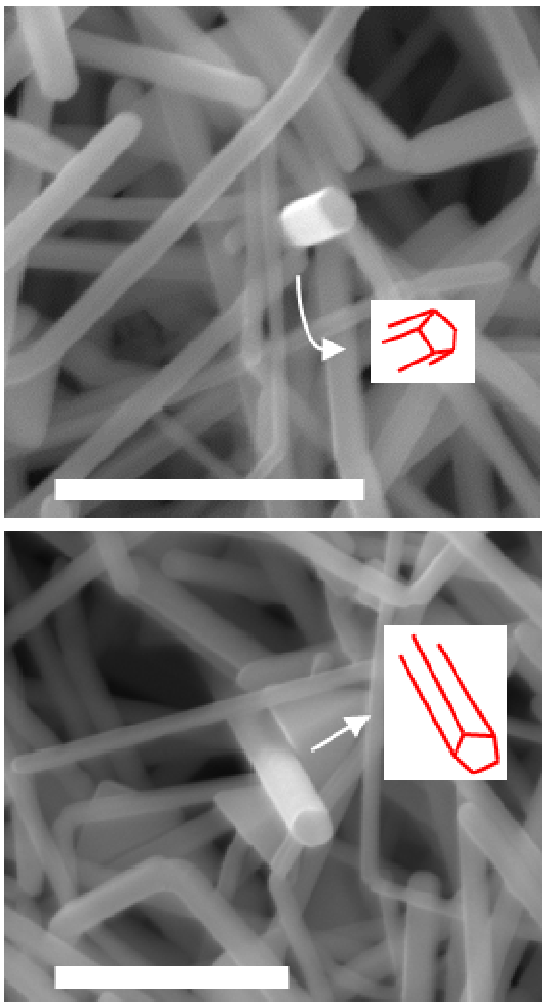

Figure A2.5 SEM images of pentagonally twinned Ag NWs. The scale bars are 1 μm.

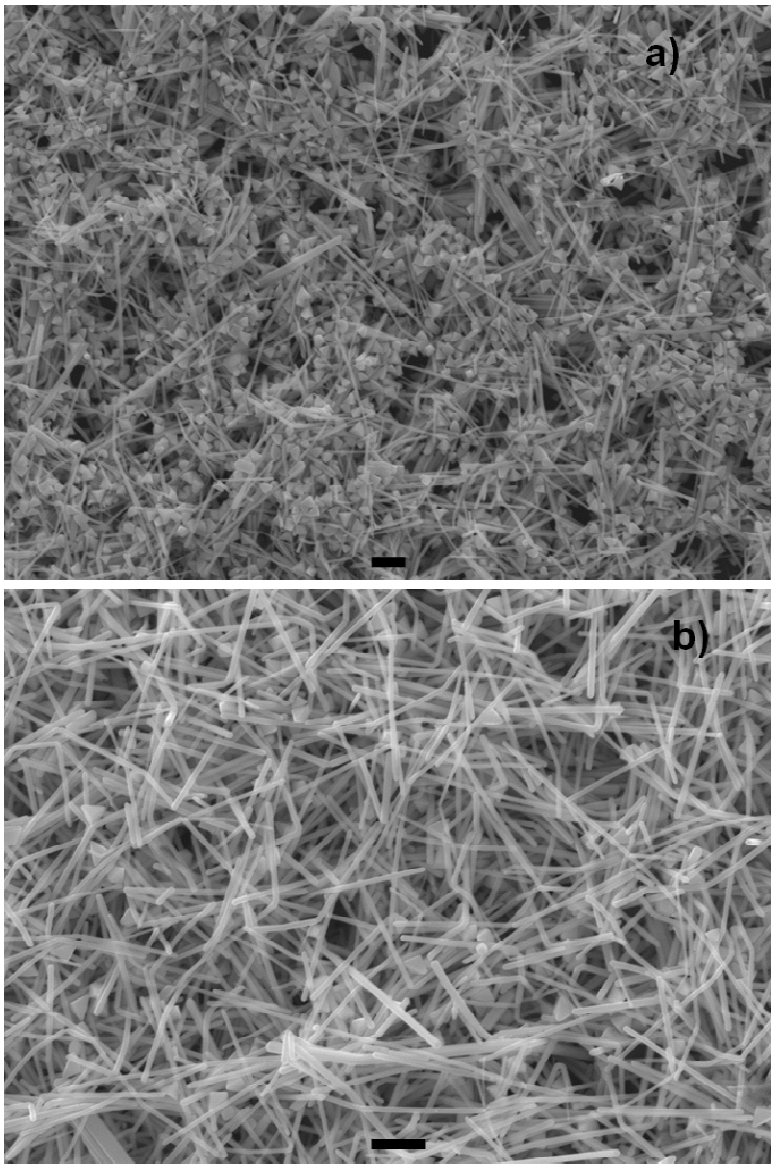

Figure A2.6 SEM images of Ag NWs a) before and b) after washing with NH_4OH. The scale bars are 1 μm.

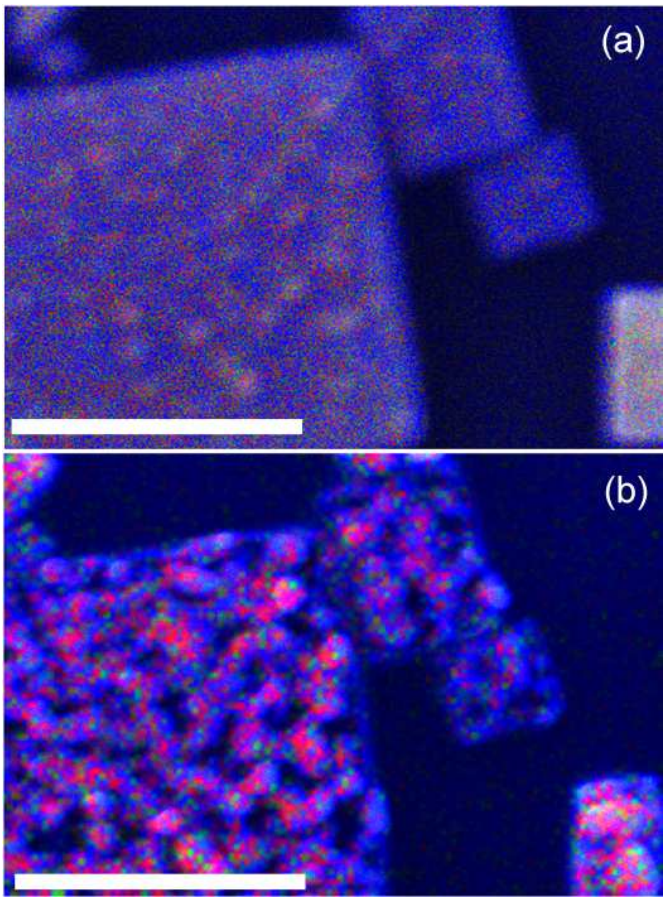

	Image a)		Image b)	
	Ag	Cl	Ag	Cl
Weight %	20.45	2.66	18.40	1.38
Atomic %	4.69	1.97	4.50	1.03

Figure A2.7 Beam damage of a representative AgCl nanocube in the SEM. Image b) was taken a few minutes after image a) was taken. Blue – the Si(111) substrate, Red – Ag, Green – Cl. The weight and atomic percentages in the table were obtained by energy-dispersive spectroscopy (EDS) in the SEM. The low absolute values reported for Ag and Cl reflect that Si from the substrate was the majority element detected by EDS. The scale bars are 1 μm.

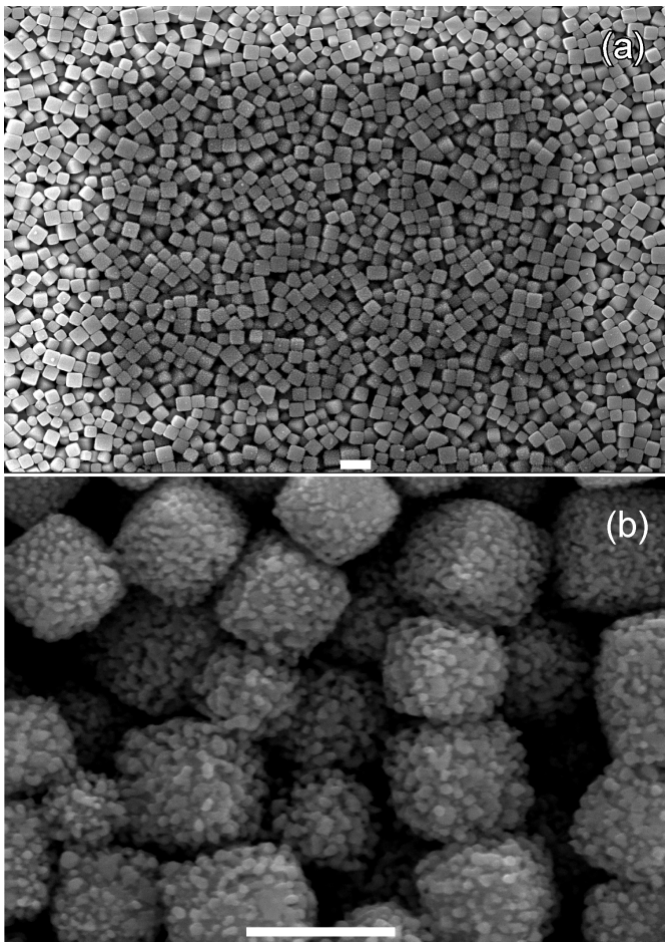

Figure A2.8 Beam damage in pre-synthesized AgCl nanocubes in the SEM. a) The darkened region was previously rastered with the e-beam prior to collecting the expanded image. AgCl nanocubes in the darkened regions have more Ag nodules on them. b) A zoomed image of the darkened region in part a. The scale bars are 1 μm.

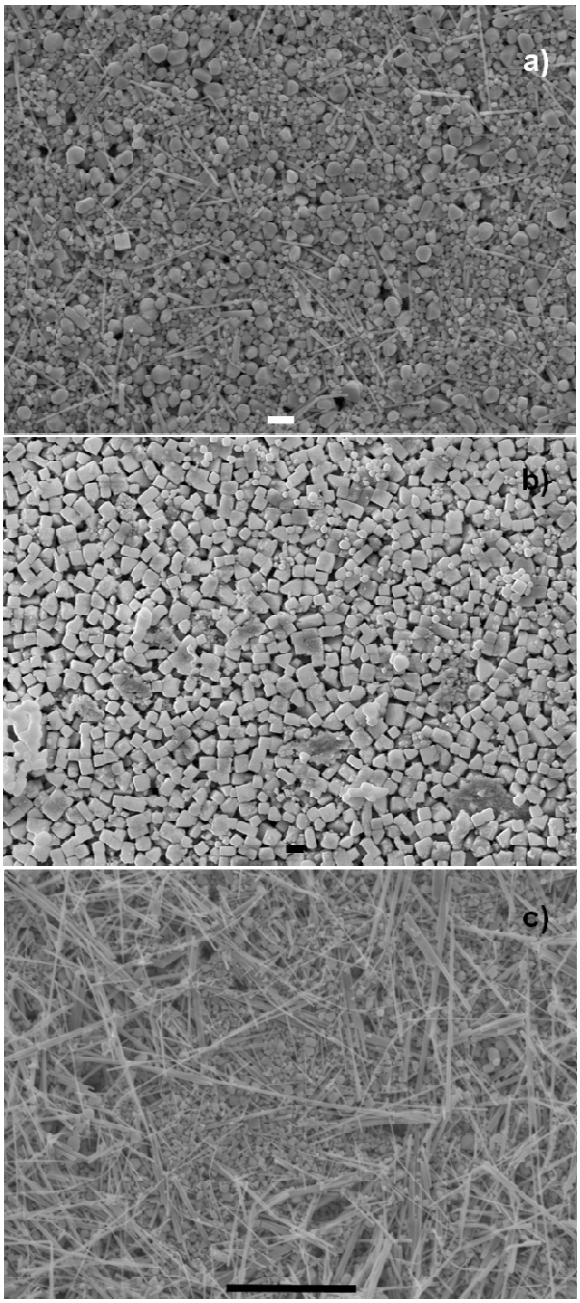

Figure A2.9 SEM images from control reactions (using ethylene glycol from Aldrich) a) lacking any chloride additive, b) omitting the second addition of $AgNO_3$ 30 min after the start of the reaction and c) starting the dropwise addition of $AgNO_3$ 7 min after the start of the reaction. The scale bar is 1 μm for a) and b) and 10 μm for c).

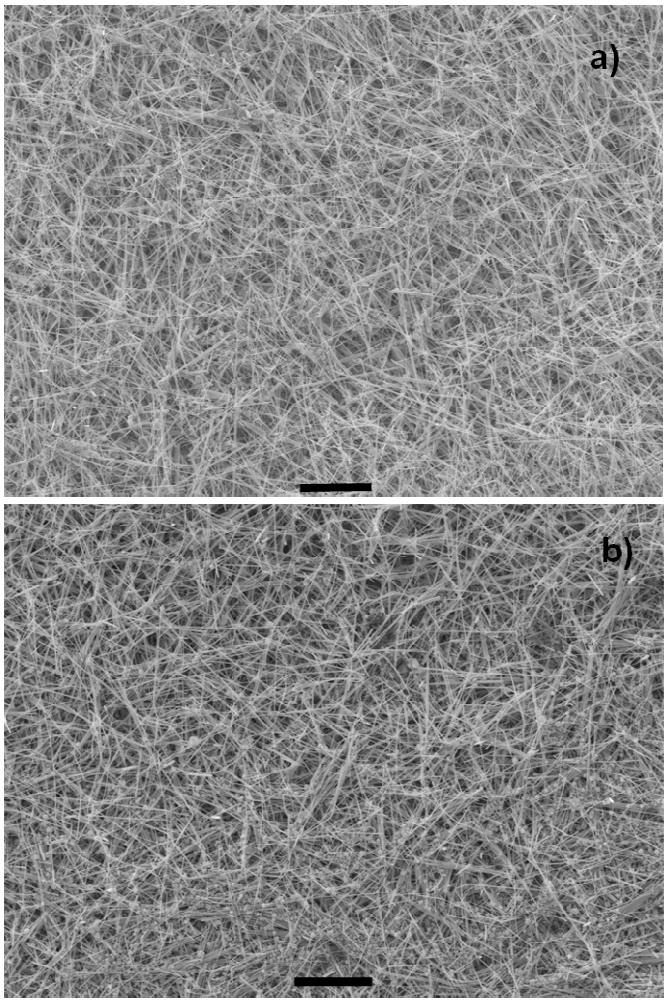

Figure A2.10 SEM images from Ag NW synthesis reactions using J. T Baker high purity ethylene glycol with a) low NaCl concentration and b) high NaCl concentration. The scale bars are 10 μm.

Appendix B

Additional Figures and Supporting Text for Chapter 3

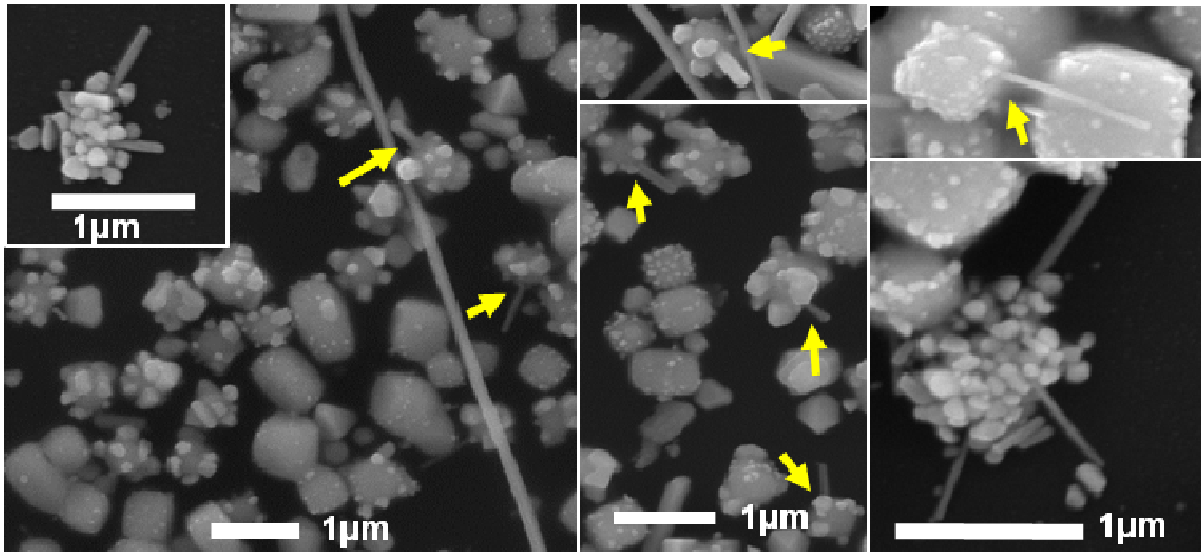

Figure B3.1 Ag NWs nucleated from pre-synthesized AgCl nanocubes (indicated by yellow arrows) at a time near initiation of wire growth.[2] The AgCl nanocubes employed here were larger (250-500 nm) than those used in current study (100 ± 31 nm).

Table B3.1 Final mean diameters and lengths recorded at various temperatures.

Temperature (°C)	Final mean diameters (μm)	Final mean lengths (μm)
150	0.07821	14.62
160	0.06042	11.94
170	0.08076	11.37
180	0.06678	9.136

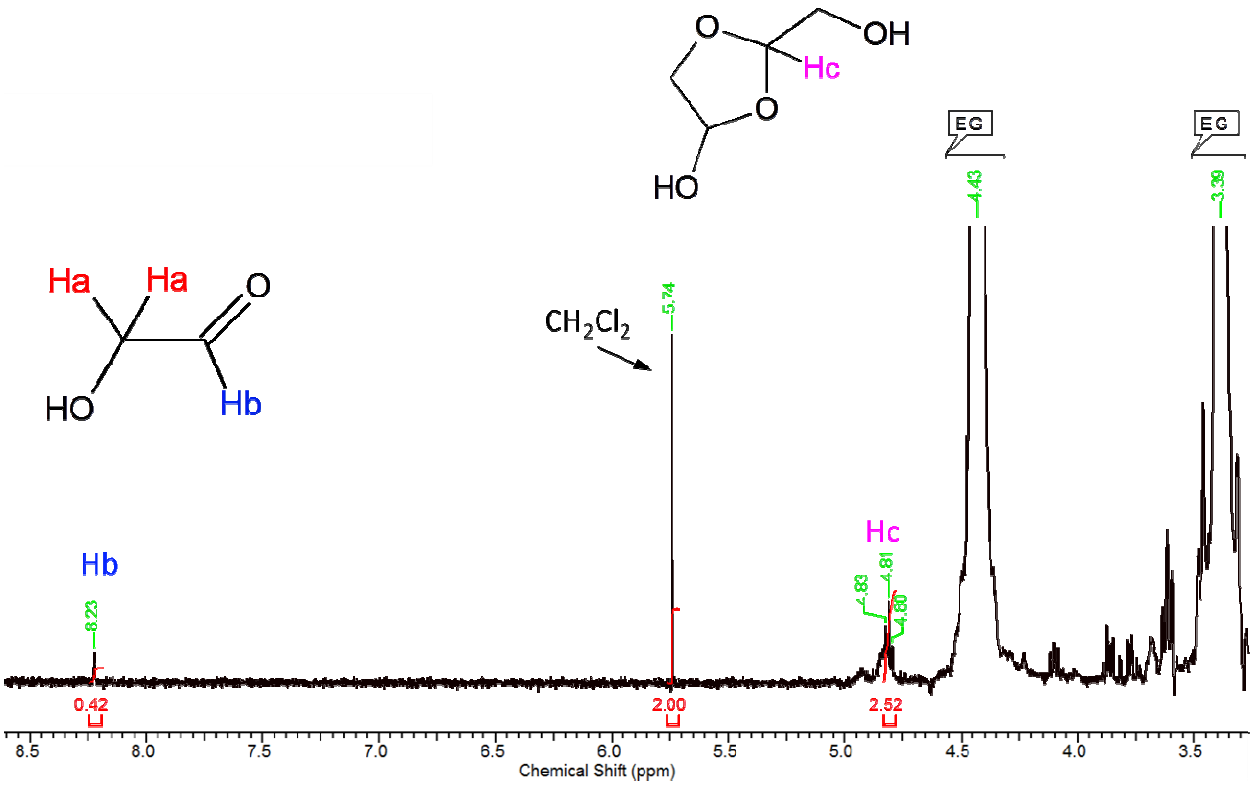

Figure B3.2 ^{1}H-NMR spectrum from the reaction of ethylene glycol and concentrated nitric acid, with methylene chloride as an internal standard in d_6-DMSO.

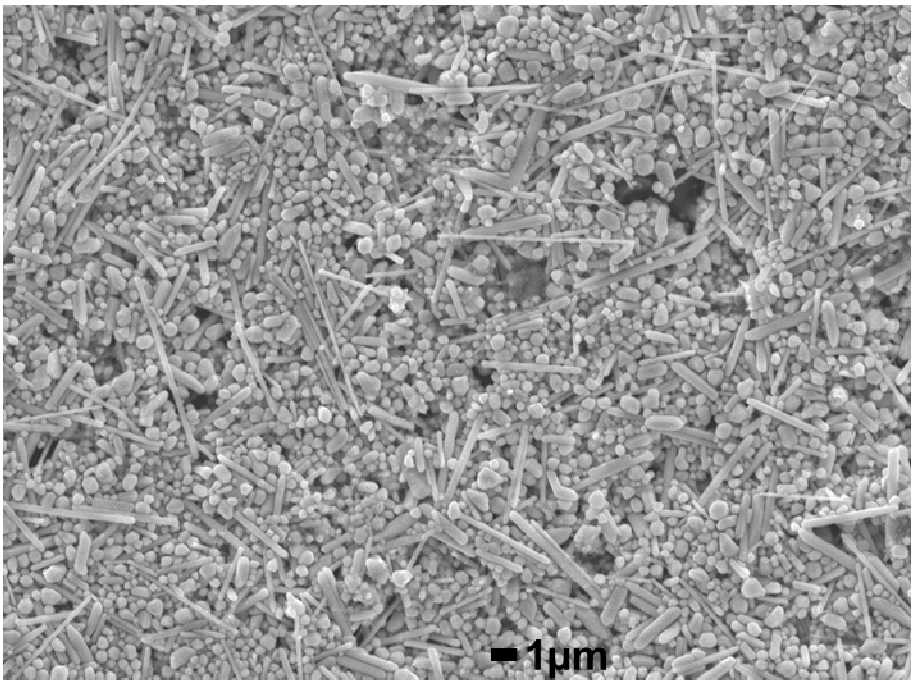

Figure B3.3 SEM image of a Ag NW synthesis at 170 ºC with added glycolaldehyde dimer.

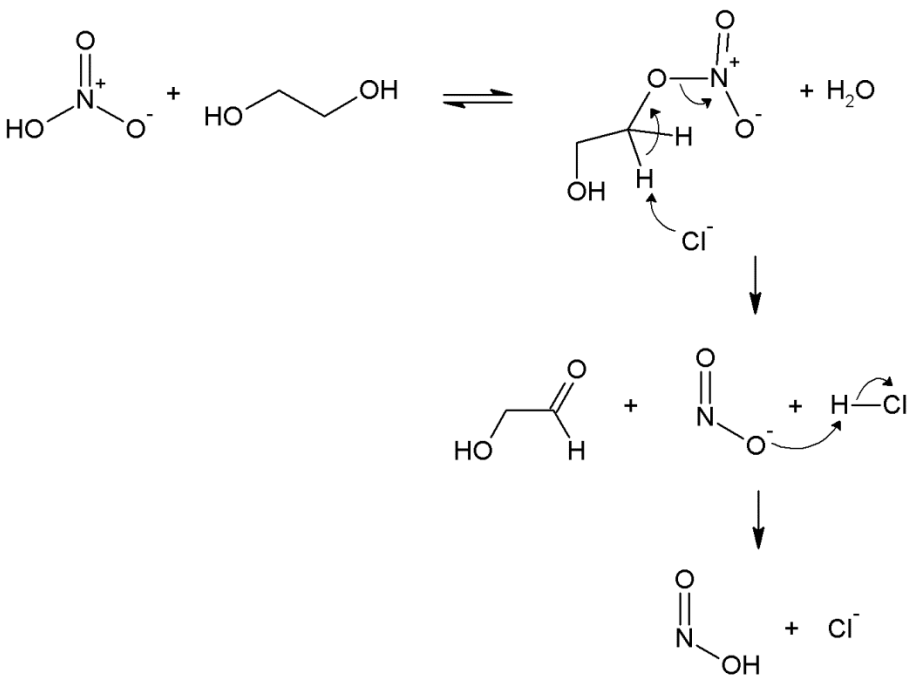

Scheme B3.1 Pathway for HNO_3 oxidation of ethylene glycol to glycolaldehyde.

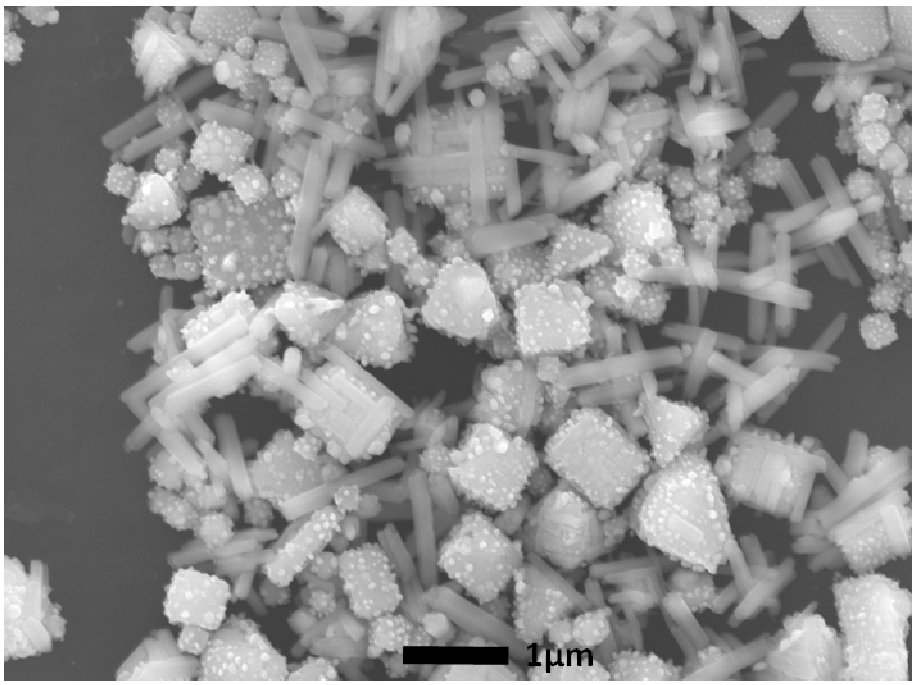

Figure B3.4 SEM image of a reaction aliquot taken 39 min into Ag NW synthesis reaction (150 ºC) with added HNO_3.

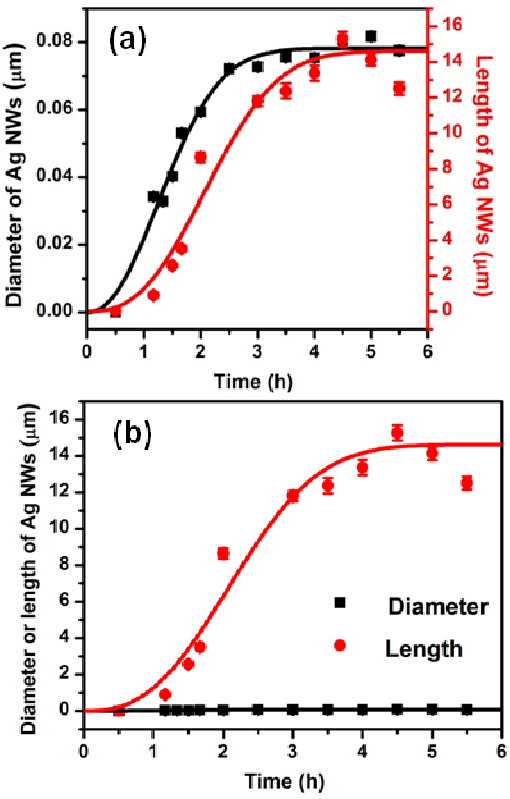

Figure B3.5 Plots of time-dependent growth in length and diameter of Ag NWs at 150 ºC on (a) relative y-axis scales and (b) an absolute (single) y-axis scale. The error bars are ± one st. error of mean in each data point. Error bars are not visible where the error is smaller than the symbol size.

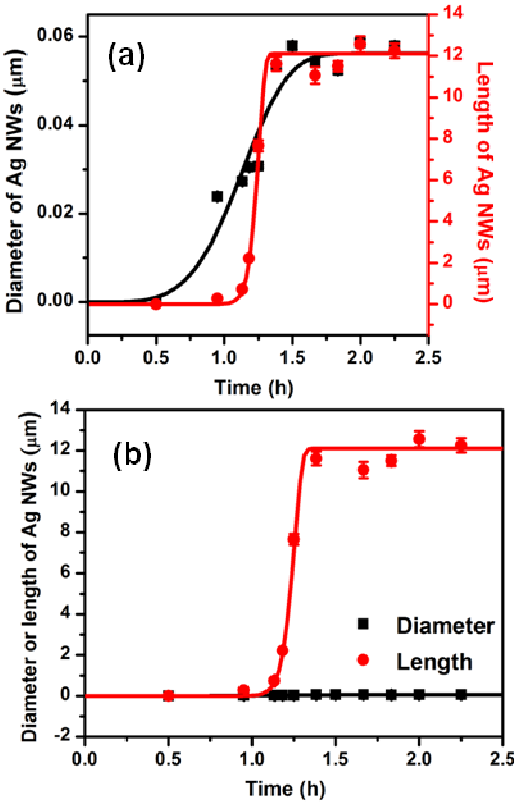

Figure B3.6 Plots of time-dependent growth in length and diameter of Ag NWs at 160 ºC on (a) relative y-axis scales and (b) an absolute (single) y-axis scale. The error bars are ± one st. error of mean in each data point. Error bars are not visible where the error is smaller than the symbol size.

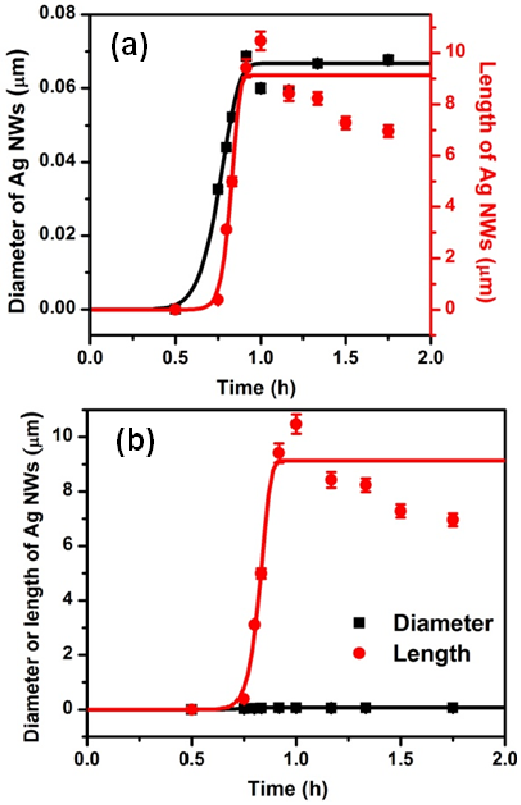

Figure B3.7 Plots of time-dependent growth in length and diameter of Ag NWs at 180 ºC on (a) relative y-axis scales and (b) an absolute (single) y-axis scale. The error bars are ± one st. error of mean in each data point. Error bars are not visible where the error is smaller than the symbol size.

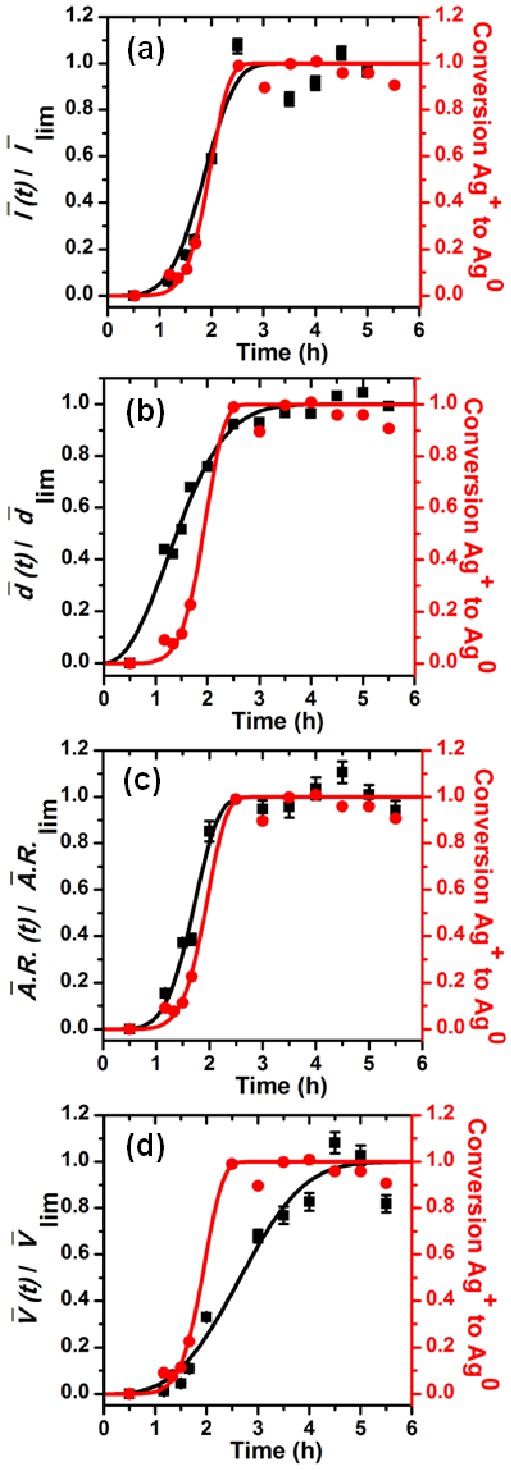

Figure B3.8 Plots of conversion of Ag^{+} to Ag^{0} with growth kinetics. Normalized mean (a) length with eq-3 fit, (b) diameter with eq-4 fit, (c) aspect ratio (AR) with the corresponding fit and (d) volume with the corresponding fit. Each of a-d includes the eq-1 fit and is plotted as a function of reaction time at 150 °C. The error bars are ± one st. error of mean in each data point. Error bars are not visible where the error is smaller than the symbol size.

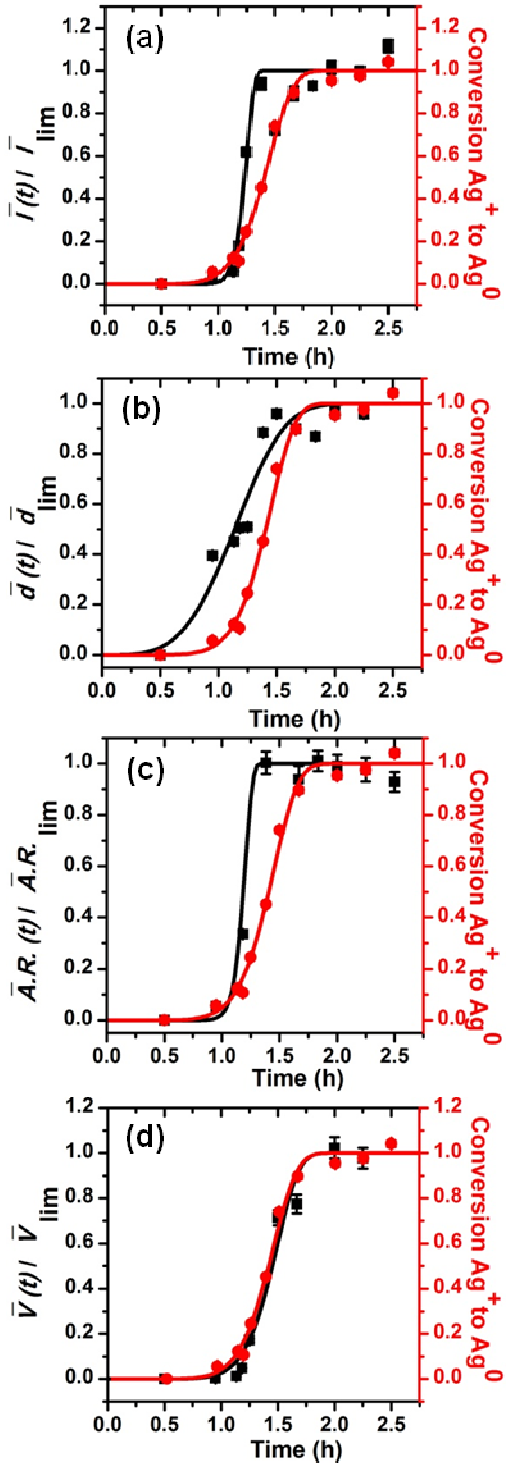

Figure B3.9 Plots of conversion of Ag^{+} to Ag^{0} with growth kinetics. Normalized mean (a) length with eq-3 fit, (b) diameter with eq-4 fit, (c) aspect ratio (AR) with the corresponding fit and (d) volume with the corresponding fit. Each of a-d includes the eq-1 fit and is plotted as a function of reaction time at 160 °C. The error bars are ± one st. error of mean in each data point. Error bars are not visible where the error is smaller than the symbol size.

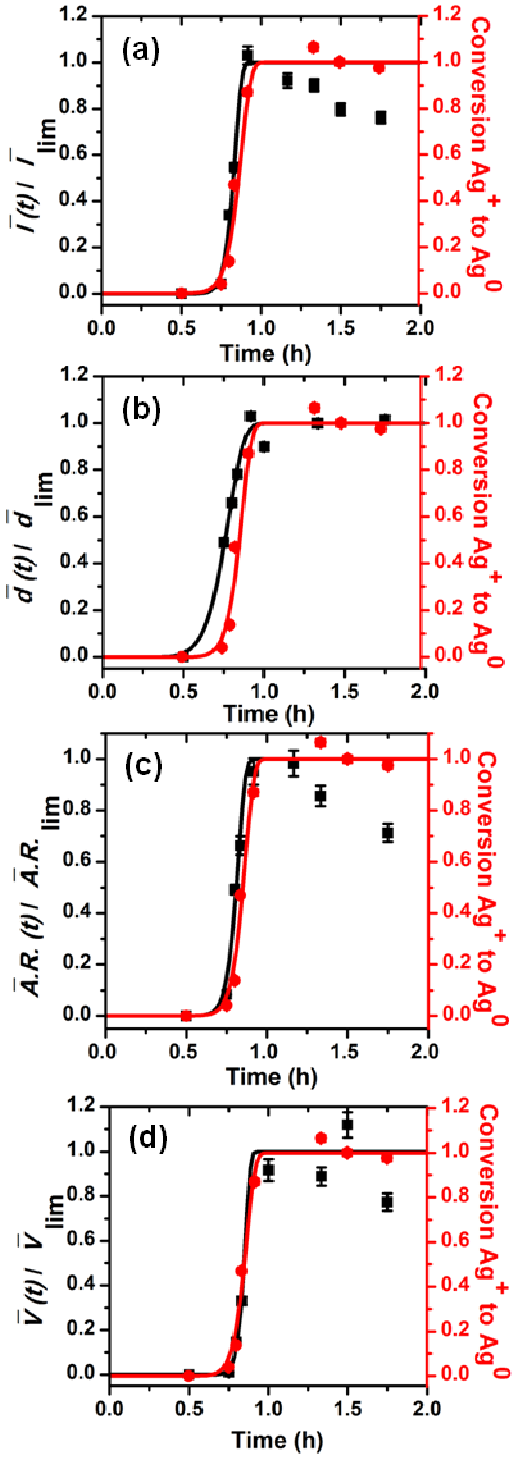

Figure B3.10 Plots of conversion of Ag^{+} to Ag^{0} with growth kinetics. Normalized mean (a) length with eq-3 fit, (b) diameter with eq-4 fit, (c) aspect ratio (AR) with the corresponding fit and (d) volume with the corresponding fit. Each of a-d includes the eq-1 fit and is plotted as a function of reaction time at 180 °C. The error bars are ± one st. error of mean in each data point. Error bars are not visible where the error is smaller than the symbol size.

B3.1 Calculation of Diffusion-Limited Rates and Experimental Reaction Rates[20]

For the steady state diffusion of Ag^+ ions towards the growing Ag NW, the maximum diffusion controlled rate constant, k_D (Table B3.2) was calculated from eq B1. The diffusion of the larger growing Ag NW is assumed to be negligible in comparison to the diffusion of the Ag^+ ions in solution.

$$k_D = 2\pi N_0 D_{Ag^+}\left(r_{Ag^+} + r_{Ag}\right) \qquad \text{(B1)}$$

Table B3.2 Temperature dependant viscosity of ethylene glycol, experimentally determined reaction rates and rate constants and calculated rate of encounter and diffusion controlled rate constants.

Temperature (°C)	**Viscosity of ethylene glycol ($\times 10^{-4}$ kg m^{-1}s^{-1})[a]**	**Diffusion Coefficient of Ag^+, D_0 ($\times 10^{-9}$ m^{2}s^{-1})**	**Diffusion controlled rate constant, k_D ($\times 10^{9}$ Lmol^{-1}s^{-1})**	**Ag^+ reduction rate constant, k_r ($\times 10^{-4}$ s^{-1})**
150	7.50	3.30	3.35	2.11
160	6.90	3.36	3.73	8.83
170	6.20	3.43	4.25	20.5
180	5.70	3.51	4.72	30.7

[a]The temperature-dependent viscosity of ethylene glycol was extracted from Figure B3.11 by fitting the viscosity vs. temperature graph[22] to an exponential decay function.

In eq B1, r_{Ag^+} and r_{Ag} are the radii of Ag^+ (1.26 Å[21]) and Ag (1.44 Å[21]), N_0 is the Avogadro's number, D_{Ag^+} is the diffusion coefficient of Ag^+ ions estimated from Stokes-Einstein equation, eq B2 (see Table B3.2) which relates the diffusion coefficient of a Ag^+ ions to the viscosity of ethylene glycol (Figure B3.11).

$$D_{Ag^+} = \frac{k_B T}{6\pi r_{Ag^+}\eta} \qquad \text{(B2)}$$

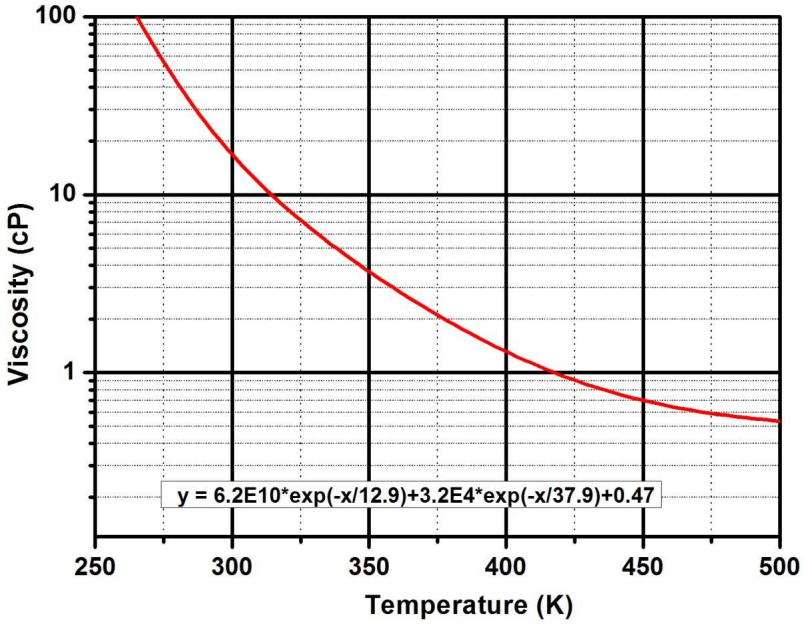

Figure B3.11 Temperature-dependent viscosity of ethylene glycol replotted from Ref. 22 and fitted with an exponential decay function.

In case of a diffusion-controlled process, the diffusion of Ag^+ ions to the surface of the growing Ag NW will be the rate-limiting step followed by a faster Ag^+ reduction reaction on the surface of the Ag NW. The rate of encounters of Ag^+ ions and Ag NWs was calculated using the following rate law (Table B3.3).

$$\text{Rate of Encounters} = k_D\,[Ag^+][Ag] \qquad \text{(B3)}$$

Table B3.3 Experimentally determined Ag^+ reduction rates and calculated diffusion-limited rates corresponding to time when the reduction reaction is 50% completed.

Temperature (ºC)	**T ½ (min)**	**Experimentally determined Ag^+ reduction rates (x 10^{-6} M/s)**	**Calculated diffusion-limited rates (x 10^{8} M/s)**
150	75.6	7.46	1.67
160	54.0	29.5	1.58
170	27.6	66.6	1.53
180	21.6	80.8	1.24

Alternatively, following the formation of an encounter pair, in the activation-controlled limit, the Ag^+ reduction reaction at the surface of the Ag NW will be the rate-limiting step. A first order

rate constant, k_r of Ag^+ reduction reaction was calculated from the slope of the linear plot of $\ln([Ag^+]/[Ag^+]_0)$ as a function of time (Figure B3.12, Table B3.2). Only the data points from the steeply rising portion of the S-shaped curve (Figure 3.3) were used in Figure B3.12. The overall rate law of the Ag^+ reduction reaction was calculated as follows (Table B3.3).

$$Ag^+ \text{ Reduction Rate} = k_r [Ag^+] \qquad \text{(B4)}$$

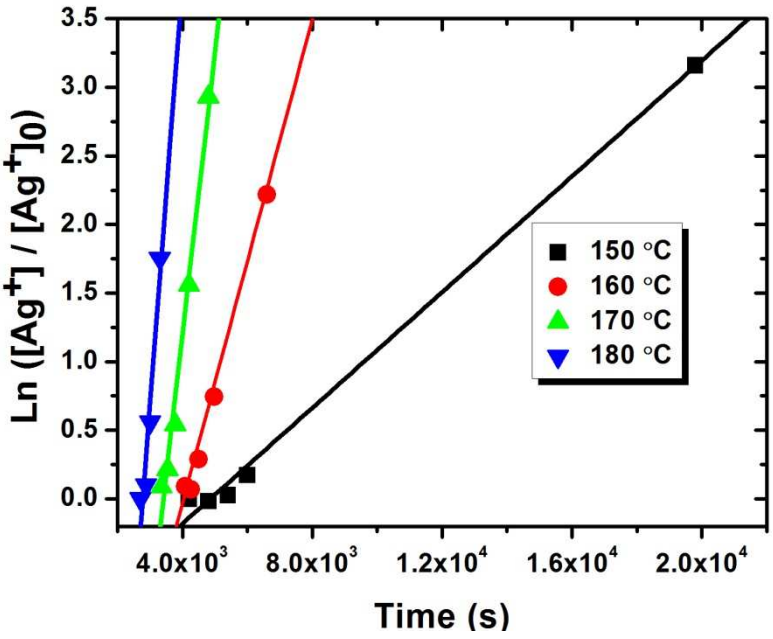

Figure B3.12 Plot of $\ln([Ag^+]/[Ag^+]_0)$ as a function of time and temperature with linear fits using the data points from the steeply rising portion of the S-shaped curves from Figure 3.3.

The Ag^+ reduction rate was calculated to be ~13 orders of magnitude slower than the rate of diffusion of Ag^+ ions to the surface of the growing Ag NW as recorded in Table B3.3.

The activation energy of the Ag^+ reduction reaction was calculated from the Eyring plot (Figure B3.13). From thermodynamics the reaction rate constant, k can be expressed as,

$$k = \frac{k_B T}{h} \exp\left(\frac{\Delta H^{\neq}}{RT}\right) \exp\left(\frac{\Delta S^{\neq}}{R}\right) \qquad \text{(B5)}$$

Rearranging the above equation and taking logarithm on both sides,

$$ln\left(\frac{kh}{k_B T}\right) = -\frac{\Delta H^{\neq}}{RT} + \frac{\Delta S^{\neq}}{R} \qquad \text{(B6)}$$

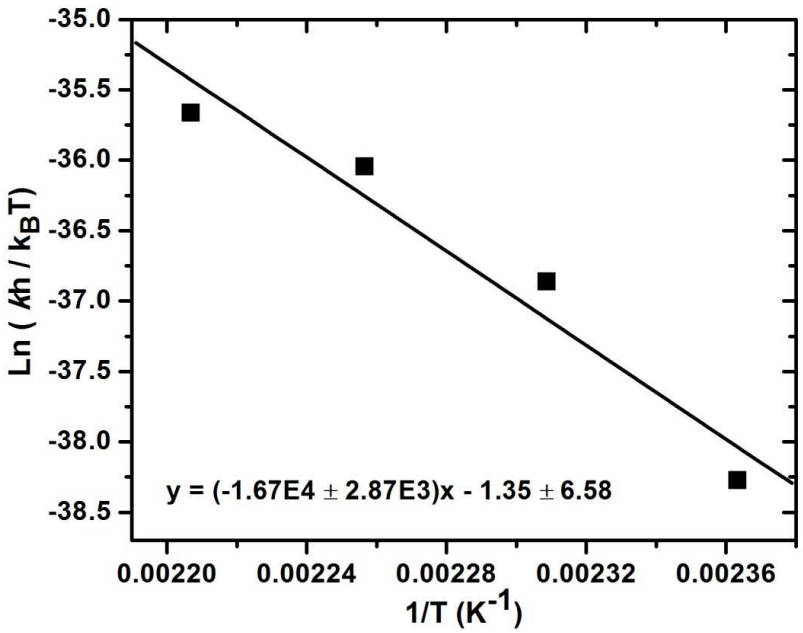

Figure B3.13 Eyring Plot using experimentally determined rate constants.

From the slope of the Eyring plot (Figure B3.13), the enthalpy of activation $\Delta H^{\neq}$ was calculated to be 138.5 kJ/mol. The entropy of activation $\Delta S^{\neq}$ was calculated from the y-intercept to be -11.2 kJ/mol. Using the $\Delta H^{\neq}$ and $\Delta S^{\neq}$ values above, eq B7 was used to calculate the activation energy of the Ag^{+} reduction reaction (138.6 kJ/mol at 423 K).

$$E_a = \Delta H^{\neq} + RT \qquad \text{(B7)}$$

B3.2 Predicting the Activation Energy for a Diffusion-Controlled Process in Ethylene Glycol[23]

The viscosity of ethylene glycol follows an Arrhenius-like temperature dependence where E_η is the activation energy for viscosity of ethylene glycol and η_0 is a constant,

$$\eta(T) = \eta_0 exp\left(\frac{E_\eta}{RT}\right) \qquad \text{(B8)}$$

Using eq B8 and viscosity values for ethylene glycol at 400 K and 500 K from Figure B3.11, E_η was calculated at 423 K to be 20.2 kJ/mol.

To calculate the expected activation energy for a diffusion-controlled reaction E_d in ethylene glycol at 423 K, the following derivation was used:

The maximum diffusion-limited rate constant for two solute molecules A and B can be expressed as follows,

$$k_D = 2\pi N_0 (D_A + D_B)(r_A + r_B) \qquad \text{(B9)}$$

The diffusion coefficient of A and B are,

$$D_A = \frac{k_B T}{6\pi r_A \eta} \; ; \; D_B = \frac{k_B T}{6\pi r_B \eta} \qquad \text{(B10)}$$

Substituting eq B8 into eq B10,

$$D_A = \frac{k_B T}{6\pi r_A \eta_0} \exp\left(\frac{-E_\eta}{RT}\right) \; ; \; D_B = \frac{k_B T}{6\pi r_B \eta_0} \exp\left(\frac{-E_\eta}{RT}\right) \qquad \text{(B11)}$$

Substituting eq B11 into eq B9,

$$k_D = 2\pi N_0 (r_A + r_B)\left(\frac{k_B T}{6\pi r_A \eta_0} \exp\left(\frac{-E_\eta}{RT}\right) + \frac{k_B T}{6\pi r_B \eta_0} \exp\left(\frac{-E_\eta}{RT}\right)\right) \qquad \text{(B12)}$$

Rearranging,

$$k_D = \frac{2N_0 k_B T}{3\eta_0} \exp\left(\frac{-E_\eta}{RT}\right) \qquad \text{(B13)}$$

Taking logarithm on both sides and differentiating w.r.t T,

$$\frac{dk_D}{dT} = d\, ln\left(\frac{2N_0 k_B}{3\eta_0}\right) + \text{dln(T)} + \text{d}\left(\frac{-E_\eta}{RT}\right) \qquad \text{(B14)}$$

$$\frac{dk_D}{dT} = \frac{1}{T} + \frac{E_\eta}{RT^2} \qquad \text{(B15)}$$

The Arrhenius temperature dependence for diffusion of solute molecules with an activation energy of diffusion E_d can be expressed as follows,

$$k(T) = Aexp\left(\frac{-E_d}{RT}\right) \qquad \text{(B16)}$$

Taking logarithm on both sides of and differentiating w.r.t T,

$$\frac{dk}{dT} = d\ln A + \mathrm{d}\left(\frac{-E_d}{RT}\right) \qquad \text{(B17)}$$

Rearranging,

$$\frac{dk}{dT} = \frac{E_d}{RT^2} \qquad \text{(B18)}$$

Equating eq B15 and eq B18,

$$\frac{E_d}{RT^2} = \frac{1}{T} + \frac{E_\eta}{RT^2} \qquad \text{(B19)}$$

Rearranging,

$$E_d = E_\eta + RT \qquad \text{(B20)}$$

Using the previously calculated value of E_η (see above), E_d was calculated to be 23.7 kJ/mol.

B3.3 References:

20. Barrow, G. M. The Nature of Chemical Reactions: Rates and Mechanisms. *Physical Chemistry*. 3rd ed.; McGraw-Hill, 1973, 419-450.

21. Mango, H. N. Silver: Element and geochemistry. *Geochemistry*. Springer Netherlands, 1998. pp 575-577.

22. Russell, D. H. Glycols: edited by George O. Curme, Jr. and Franklin Johnston. New York, Reinhold Publishing Corp., 1953; 84.

23. Roussel, M. R. Diffusion and reactions in solution. *A life scientist's guide to physical chemistry*. Cambridge University Press. 2012; 359-374.